The sedimentary record of ultrahigh-pressure metamorphism: a perspective review

Jan Schönig[1*], Hilmar von Eynatten[1], Guido Meinhold[1,2,3], Nils Keno Lünsdorf[1]

[1]Department of Sedimentology and Environmental Geology, Geoscience Center Göttingen, University of Göttingen, Goldschmidtstraße 3, 37077 Göttingen, Germany

[2]School of Geography, Geology and the Environment, Keele University, Keele, Staffordshire, ST5 5BG, UK

[3]Institute of Geology, TU Bergakademie Freiberg, Bernhard-von-Cotta-Straße 2, 09599 Freiberg, Germany

[*]corresponding author: jan.schoenig@uni-goettingen.de

Abstract

Tracing ultrahigh-pressure (UHP) metamorphism of crustal rocks through the geological record is a key for understanding the evolution of plate tectonics on Earth due to the linkage with deep subduction processes. Until recently, UHP research was almost exclusively based on the investigation of crystalline rocks, but findings of coesite and diamond inclusions in detrital mineral grains demonstrate that the sedimentary record archives mineralogical evidence for UHP metamorphism. We here review previous attempts to link sediments to UHP sources and the recent findings of detrital UHP garnet, and thoroughly discuss the new approach in the search for UHP metamorphism. The indicative UHP minerals were identified by Raman spectroscopy and include monomineralic coesite and bimineralic coesite + quartz inclusions in detrital garnets from the Scandinavian Caledonides of Norway, the D'Entrecasteaux Metamorphic Complex of Papua New Guinea, and the Central European Variscides of Germany, as well as diamond inclusions in the latter. Garnet chemistry and inclusion assemblages are used to gain information about the origin of these mineral grains and to discriminate different UHP sources. Presumably, the value of information will increase in future studies by considering other

detrital containers of UHP minerals such as the ultrastable heavy minerals zircon, rutile, and tourmaline, for which also a range of single-grain provenance tools exist. Abundant monomineralic coesite inclusions in detrital minerals allow for investigating coesite preservation factors and potentially elastic thermobarometry in the coesite stability field. Altogether, the method allows for (i) screening large regions systematically for the presence of UHP rocks, (ii) studying the exhumation history of UHP terranes, and (iii) monitoring the former existence of UHP terranes at the Earth's surface.

Keywords: Ultrahigh-pressure metamorphism; mineral inclusions; detritus; provenance; Raman spectroscopy; coesite; diamond; garnet; ultrastable minerals.

1. Introduction

Ultrahigh-pressure (UHP) metamorphism of continental crust is intimately connected to deep (>100 km) subduction processes (e.g. Chopin, 2003), which are characteristic of modern-style plate tectonics (e.g. Stern, 2005). Tracking these processes through the geological record is of first-order significance in Earth sciences to draw conclusions on the evolution of subduction tectonics in Earth history. Although several mineralogical indicators have been proposed and were controversially discussed, the best and unequivocal indicators for UHP metamorphism are inclusions of coesite and diamond in mechanically robust host minerals (e.g. Chopin, 2003; Kotková et al., 2011). This is well known since the breakthrough studies in the 1980s reporting bimineralic coesite + quartz inclusions in garnet and omphacite (Chopin, 1984; Smith, 1984), and diamond inclusions in garnet of crustal rocks in the early 1990s (Sobolev and Shatsky, 1990). Since then, a great number of terranes have been identified that experienced deep subduction processes and were subsequently exhumed, making UHP metamorphism a common phenomenon in Earth's metamorphic record since the late Neoproterozoic (Liou et al., 2009).

Studies identifying UHP metamorphism are primarily based on the investigation of crystalline rocks, and approaches using the sedimentary record to constrain the erosion of UHP rocks are extremely scarce. The few studies available are sedimentary provenance studies, where chemical and

isotopic characteristics of detrital single grains are roughly linked to the characteristics of known UHP terranes, which could represent a potential source of the sediments (e.g. Grimmer et al., 2003; Li et al., 2005). These techniques, however, are unable to verify UHP sources or explore regions on the existence of these rocks. The identification of coesite inclusions in zircons of cobbles from conglomerates (Wan et al., 2005) is restricted to coarse clastic sediments, and thus this technique is only suitable in certain circumstances, such as in proximal settings. In contrast, in an individual case, coesite inclusions were reported from single detrital zircon grains (Chen et al., 2005). Recently, a novel method has been developed using Raman spectroscopy to systematically screen detrital mineral grains on the presence of coesite inclusions with a focus on garnet, which allows to pinpoint an UHP origin (Schönig et al., 2018a). This approach was first successfully applied on detrital garnet from the Western Gneiss Region of Norway and proof of concept has been demonstrated by application to modern sand samples from the Saxonian Erzgebirge of Germany (Schönig et al., 2019, 2020) and Earth's youngest UHP terrane in Papua New Guinea (Baldwin et al., 2021). In addition to common inclusions of coesite in detrital garnets of the Erzgebirge, diamond inclusions were also detected.

In this paper, we review early attempts to link sediments to UHP sources, the recent findings of UHP mineral inclusions in detrital garnet, and the related method of capturing the distribution and characteristics of UHP metamorphic rocks by combining mineral inclusion data with garnet chemistry. This also includes the benefits as well as challenges, which have to be carefully considered, and the prospective enhancements of the method. Furthermore, we discuss the potential of detrital UHP host minerals beyond garnet, with particular emphasis on heavy minerals which are ultrastable within the sedimentary cycle. Finally, we give an outlook on fields of application by considering the sedimentary record as an archive for UHP metamorphism.

2. Attempts to link sediments to UHP sources

Early attempts to link sedimentary successions to the erosion of UHP source rocks are restricted to the Dabie Shan and Sulu terranes located in the eastern part of the Qinling–Dabie–Sulu Orogen in China (Fig. 1A). The UHP rocks in this orogen were formed during collision of the North and South

China blocks in the Triassic (Li et al., 2005). To evaluate the timing of exposure, sedimentary rocks of various basins surrounding the Qinling–Dabie–Sulu Orogen were considered to be sourced from the Dabie and Sulu UHP rocks.

[insert Figure 1, two-column fitting image]

Considerable attention has been given to the large volumes of Triassic turbidites of the Songpan–Ganzi Complex located ~1000 km west of the present-day outcropping UHP rocks of the Dabie Shan (Fig. 1A). By comparing the age and volume of the Songpan–Ganzi Complex with the amount of material proposed to have overlain the Dabie UHP rocks, Nie et al. (1994) proposed that the majority of the Triassic sediments were sourced from the eroding Qinling–Dabie Orogen during exhumation of the UHP rocks. Besides possible pitfalls in this mass balance attempt, doubts on this interpretation have been raised due to the missing mineralogical evidence for the contribution of eroded material from both UHP and the formerly overlying high-pressure (HP) rocks (Avigad, 1995). Later, detrital zircon U–Pb ages revealed that the Songpan–Ganzi Complex consists of multiple depocenters with different sources and that low Th/U detrital zircons, which are typical for the UHP rocks from Dabie as well as metamorphic zircon in general (e.g. Rubatto, 2017, and references therein), show different ages than their supposed source rocks (Weislogel et al., 2006, 2010). Yet, the sediment sources of the Triassic turbidites of the Songpan–Ganzi Complex are still a matter of debate; various sources are proposed including the Dabie UHP rocks, the Qinling–Dabie Orogen, Qaidam Block (Kunlun Arc), the South China Block, the Qiantang UHP rocks, and the Qiantang Block (e.g. Zhang et al., 2012, and references therein, Fig. 1A). Studies suggesting the presence or absence of an UHP source are based on the occurrence of HP minerals like omphacite, the chemical composition of garnet, a high Si content in white mica, and comparison of zircon U–Pb or white mica $^{40}Ar/^{39}Ar$ ages with supposed UHP source terranes (e.g. Enkelmann et al., 2007; Zhang et al., 2008).

In contrast to the supposed long transport to the Songpan–Ganzi Basin, Grimmer et al. (2003) assume deposition of erosional material sourced from the Dabie UHP rocks in closer proximity in the Yangtze foreland, located south-east of the Dabie UHP terrane (Fig. 1A). To link the investigated

sediments to a Dabie source, they compared $^{40}Ar/^{39}Ar$ ages of white mica. Because a few of these micas in the Middle Jurassic successions show high Si values of >3.5 apfu (atoms per formula unit, O = 11), the authors propose a first limited exposure of Dabie UHP rocks at this time.

In addition, it is also considered that eroded material from the Dabie UHP rocks was accumulated in the Hefei Basin (Fig. 1A). Li et al. (2005) recognized a prominent change in the Si content of white mica within the Lower Jurassic Fanghushan Formation from dominantly <3.3 apfu to dominantly >3.3 apfu. This trend continues in the younger formations. Based on the Triassic age of some zircons, the authors link the Lower Jurassic sediments to a Dabie source. Most convincingly, evidence for the exposure and erosion of UHP rocks is given by coesite inclusions in detrital zircon from sandstone of the Fanghushan Formation (Chen et al., 2005) and also by coesite inclusions in zircon of a granitic gneiss cobble from an Upper Jurassic conglomerate of the Fenghuangta Formation (Wan et al., 2005).

A similar approach of comparing chemical composition and U–Pb ages of detrital zircon with a known UHP terrane was performed by Xie et al. (2012). The authors analyzed zircons from the Lower Cretaceous Laiyang Group of the Jiaolai Basin (Fig. 1A), which is adjacent to the Sulu UHP terrane that in turn is supposed to be the eastern extension of the Dabie UHP terrane (e.g. Hacker et al., 1998). Because the analyzed zircons show low Th/U ratios, indicating a metamorphic origin, and U–Pb ages similar to those of metamorphic rocks of the Sulu terrane, UHP rocks of the latter are proposed as sediment source and thus were probably exposed on the Earth's surface during early Cretaceous time (Xie et al., 2012).

As outlined by the provenance studies from sedimentary basins in China, attempts to trace UHP metamorphism through the sedimentary record are mainly based on mineral chemical composition of mica and rarely garnet, and the comparison of chronologic ages from detrital mineral grains and known potential UHP source rocks. Although determining the Si content of white mica is an important tool in sedimentary provenance analysis because the substitution of Si + (Mg, Fe) for two Al strongly depends on pressure conditions (e.g. Massonne and Schreyer, 1987), it is not possible to confidently discriminate HP and UHP sources due to the absence of information regarding the original host-rock mineral assemblage. Similarly, garnet composition is useful to identify different metamorphic sources,

but UHP garnet does not show a unique composition clearly differing from that of HP garnets (Krippner et al., 2014; Tolosana-Delgado et al., 2018; Schönig et al., 2021a). Chronologic ages of single grains are useful to obtain information about the source regions, but discriminating HP and UHP source rocks from the same region is not resolvable.

Thus, techniques to identify UHP metamorphism in the detritus are limited to mineralogical indicator phases, whereby coesite and diamond are the most important. Ideally, these minerals do not occur as single grains but show some paragenetic context of their source rock. Otherwise, a differentiation between UHP metamorphism of crustal rocks and a mantle origin (i.e. peridotites, pyroxenites, mantle eclogites, or kimberlites) is open for interpretation (e.g. Kueter et al., 2016). In addition, shock metamorphism resulting from impact events represent another formation environment of coesite (e.g. Chao et al., 1960). Thus, a coesite inclusion in zircon of a cobble-sized clast like reported by Wan et al. (2005) is exceptionally beneficial because very coarse clastic material can provide important source rock information (e.g. Cuthbert, 1991; Dunkl et al., 2009; Kellett et al., 2018). However, these gravel-sized clasts are usually a feature of proximal sedimentary successions which do not represent the majority of clastic sediments and sedimentary rocks. In contrast, sand-sized grains are widespread in modern as well as ancient clastic sediments and sedimentary rocks and can be easily analyzed by a wide range of analytical techniques, making it the preferred grain-size range in single-grain provenance analysis (e.g. von Eynatten and Dunkl, 2012). Consequently, the identification of UHP mineral inclusions in detrital single grains, as reported by Chen et al. (2005), is the most promising attempt to trace UHP metamorphism through the sedimentary record.

3. UHP mineral inclusions in detrital garnet

As outlined above, the detection of coesite and diamond inclusions in detrital mineral grains is the most desirable method to trace UHP metamorphism through the sedimentary record. Although a first report of coesite in detrital zircon was given by Chen et al. (2005), and the findings were subsequently used by Li et al. (2005), a first detailed report of a technique to systematically trace UHP metamorphism at the catchment scale by analyzing inclusions in detrital garnet was given by Schönig

et al. (2018a), and further developed and verified by Schönig et al. (2019, 2020, 2021b) and Baldwin et al. (2021).

3.1. Documented findings

3.1.1. Western Gneiss Region of Norway

Schönig et al. (2018a) analyzed 732 garnets from a modern sand sample taken at the beach at the mouth of a small stream on the south-eastern coast of the island of Runde, located in the Sorøyane UHP domain of the Western Gneiss Region in south-west Norway (Fig. 1B). This sample represents a relatively small present-day catchment of ~1 km^2. The analyzed grain-size range of very-fine to medium sand was split into the three fractions 63–125 µm, 125–250 µm, and 250–500 µm. The garnets were mounted in epoxy, grounded with SiC, polished with Al_2O_3, and the inclusions were analyzed by Raman spectroscopy.

Detrital garnets containing inclusions ≥2 µm are common in the sample (>80 %). In contrast to many other analytical *in-situ* techniques that are limited to the polished surface, Raman spectroscopy enables inclusion analysis in the entire grain volume. A total of 13 coesite inclusions were detected in six of the analyzed garnet grains, being the first report of coesite inclusions in detrital garnet single grains and directly reflecting an UHP source. These coesite inclusions are most abundant in garnets of the 63–125 µm fraction, less common in the 125–250 µm fraction, and absent in the 250–500 µm fraction.

All detected coesite inclusions are small (<12 µm, longest axis in plane view), mainly spheroidal to spherical in shape, and preserve residual strains resulting from the entrapment at UHP conditions and differential thermoelastic properties of the garnet host and the entrapped coesite. In addition, all coesite inclusions are monomineralic, and thus they lack the typical petrographic structures of bimineralic coesite + quartz inclusions resulting from the partial coesite-to-quartz transformation, like radial fracturing of the host garnet (Fig. 2A).

[insert Figure 2, two-column fitting image]

3.1.2. Saxonian Erzgebirge of Germany

By applying the analytical concept of Schönig et al. (2018a) to seven modern sand samples from tributaries draining the central part of the Saxonian Erzgebirge in Germany (Schönig et al., 2019), the method of tracing UHP metamorphism by analyzing detrital garnet was tested for present-day catchments ranging from sizes as small as Runde (~1 km^2; Schönig et al., 2018a), over catchments being up to ten times larger, and finally to a regional river catchment draining an area >500 km^2. One-hundred inclusion-bearing garnets per sample (700 grains in total) from the 125–250 µm grain-size fraction were analyzed by Schönig et al. (2019). In a follow-up study, inclusion analysis of each sample was extended to 100 garnet grains from the 63–125 µm as well as the 250–500 µm grain-size fractions (Schönig et al., 2020). Out of the 2100 studied grains, 93 garnets were identified that contain a total of 193 coesite inclusions. This includes garnet grains from all studied catchments, showing that UHP rocks in the Erzgebirge are more common and more widely distributed than previously expected.

A detailed investigation of the coesite inclusions by Schönig et al. (2021b) using hyperspectral two-dimensional Raman imaging revealed that small coesite inclusions <9 µm are primarily monomineralic, mainly spherical to spheroidal in shape with few inclusions showing sharp edges (Fig. 2A), and preserve residual strains, which is in line with observations from Norway (Schönig et al., 2018a). Rarely, small inclusions partially transformed to quartz, particularly when these are connected to fractures from other inclusions or when they are located very close to the garnet surface. In contrast, larger inclusions often partially transformed to quartz (Schönig et al. 2021b; Fig. 2B). This size dependence is a general trend that is also observed in single grains containing multiple inclusions of small monomineralic coesite and larger bimineralic coesite + quartz (cf. figs. 10 and 11 in Schönig et al., 2021b). The replacement of coesite by quartz is observed to start at the inclusion-host boundary and progresses towards the inclusion center. Occasionally, the bimineralic inclusions show a filigree of fine fractures spreading into the host garnet (Fig. 2B). As fluid availability is crucial for the coesite-to-quartz transformation (e.g. Liu and Zhang, 1996; Mosenfelder and Bohlen, 1997; Mosenfelder et al., 2005; Liu et al., 2017; Wang et al., 2018), this led to the conclusion that inclusion size is the most important factor controlling the potential of the inclusion to fracture the host garnet, and thus enable

fluid infiltration (Schönig et al., 2021b). Carbonaceous material detected at host-inclusion boundaries of bimineralic and fractured inclusions record peak temperatures of ~330°C based on the Raman thermometer of Lünsdorf et al. (2017), indicating that fracturing and fluid infiltration is a late process during exhumation (Schönig et al., 2021b). The size dependence is probably related to the initial fracture length, that is the length of the inclusion–host boundary which is defined by inclusion size (Whitney et al., 2000). Large and small inclusions entrapped in the same garnet and at the same pressure–temperature (*P*–*T*) conditions develop similar non-lithostatic inclusion strains during exhumation, but larger inclusions have a larger initial fracture length, which requires less stress to propagate into the host garnet (Schönig et al., 2021b).

Besides coesite, a total of 145 diamond inclusions were found in 54 detrital garnets of two samples (Schönig et al., 2019, 2020). Almost all (53 of 54 diamond-bearing garnets) are from a sample taken very proximal to felsic diamond-bearing rock lenses (e.g. Nasdala and Massonne, 2000), while one diamond-bearing grain was detected in the sample that represents the regional river catchment. Because the latter encompasses the known diamond-bearing rock lenses, this finding does not necessarily point to another diamond-bearing source (Schönig et al., 2020).

Diamond-bearing inclusions are up to 30 µm in dimension and mainly show an irregular shape. Some of them are monomineralic but most diamonds occur in polyphase inclusions together with varying amounts of minerals like quartz, plagioclase, graphite, rutile, apatite, and phyllosilicates (Fig. 2C). Particularly the co-existence with quartz + feldspar + phyllosilicates indicate the entrapment as a melt, which agrees with the many other melt inclusions found in the detrital garnets that sometimes include rare polymorphs like cristobalite, kokchetavite, and kumdykolite (Schönig et al., 2020). The reported diamonds represent the first record of diamond-grade UHP metamorphism of crustal rocks by analyzing the detritus, and shows that evidence of diamond-bearing UHP metamorphic rocks is reliably transferred to the sedimentary record (Schönig et al., 2019).

3.1.3. D'Entrecasteaux Islands of Papua New Guinea

The D'Entrecasteaux metamorphic complex in eastern Papua New Guinea records the youngest UHP rocks exposed on Earth's surface (Baldwin et al., 2008), dated to be of late Miocene age (e.g. Monteleone et al., 2007; Baldwin et al., 2012). However, direct mineralogical evidence for UHP metamorphism in form of coesite is restricted to a single eclogite lens (Baldwin et al., 2008; Faryad et al., 2019; Osborne et al., 2019). As further attempts to find coesite in crystalline rock samples have been unsuccessful, Baldwin et al. (2021) considered the detrital garnet record as a potential archive, similar to the approach applied in Norway and Germany (Sections 3.1.1. and 3.1.2.). The authors studied the inclusion assemblage of 354 sand-sized detrital garnets from a modern beach placer. Two coesite-bearing grains were identified, one showing a monomineralic coesite inclusion (Fig. 2A) and one showing a coesite inclusion that partially transformed to quartz (Fig. 2B). These findings substantially increased the evidence for UHP metamorphism in the actively exhuming metamorphic complex and demonstrates that the detrital garnet record is capable to trace sparsely preserved UHP relicts at the catchment scale.

3.2. UHP source rock reconstruction using garnet chemistry and inclusion assemblages

3.2.1. Verifying a subduction-related crustal origin

Although inclusions of coesite and diamond serve as powerful indicators for UHP conditions, it must be considered that their formation is not restricted to deep subduction of crustal rocks. Both coesite and diamond also occur in rocks that experienced shock metamorphism during impact events (e.g. French and Koeberl, 2010, and references therein) as well as in rocks of mantle origin (e.g. Smyth and Hatton, 1977; Schulze et al., 2000). Most mantle rocks are transported to Earth's surface as xenoliths by alkaline volcanism, i.e. by kimberlites and lamproites (e.g. Field et al., 2008). In addition, fragments of mantle rocks are emplaced into subducting continental crust at convergent plate margins and are subsequently exhumed together with their crustal country rocks (e.g. Medaris, 1980). Though this process is subduction related, the crustal rocks and intruded mantle rocks often do not share a joint *P–T* path, and mantle rocks may originate from much greater depth than reached by the subducted and exhumed slab (e.g. Spengler et al., 2006). Thus, to link detrital coesite- and diamond-bearing garnet to

the deep subduction of crustal rocks, both an impact-related origin as well as a mantle origin have to be excluded.

Impact-related coesite and diamond typically do not occur as inclusions in garnet. Furthermore, coesite of shock origin often occurs in diaplectic quartz glass, at grain boundaries, in symplectites, and/or in association with planar deformation features (e.g. Ferrière and Osinski, 2012), whereas diamond of shock origin often shows preferred crystal orientation and is associated with lonsdaleite and/or silicon carbide (Vishnevsky and Raitala, 2000). By contrast, features of coesite- and diamond-bearing mantle and crustal garnet are similar and challenging to discriminate. A first look on the heavy mineral suite of a sediment sample can provide hints whether detritus supplied from mantle rocks has to be considered, for example by the presence of chrome spinel (e.g. Nowicki et al., 2007). The chemical composition of chrome spinel can further be used as a petrogenetic indicator (Irvine, 1967; Dick and Bullen, 1984; Cookenboo et al., 1997; Mange and Morton, 2007; Han et al., 2019), but mantle and crustal chrome spinel show large compositional overlap (Gurney and Zweistra, 1995). More indicative is the major-element composition of the detrital garnet grains that entrapped coesite and diamond inclusions. Mantle garnet of ultramafic host-rock composition can be confidently identified by comparatively high Cr_2O_3 content as well as high MgO content compared to FeO_{total} (Schulze, 2003; Grütter et al., 2004; Tolosana-Delgado et al., 2018). However, particularly challenging is the discrimination of chromium-poor mantle garnet, mainly originating from mantle eclogites, and crustal eclogite-facies garnet (Hardman et al., 2018).

Two multivariate discrimination schemes are available that enable the distinction of chromium-rich as well as chromium-poor mantle garnet from crustal garnet (Hardman et al., 2018; Schönig et al., 2021a). Figure 3 shows the discrimination results of these schemes for the detrital coesite- and diamond-bearing garnet grains. Both approaches assign the majority of the detrital UHP garnet grains to a crustal origin with >98 % (Fig. 3A) and >97 % (Fig. 3B), respectively. Only a minor portion of coesite-bearing garnet grains from the Saxonian Erzgebirge are assigned to be derived from mantle rocks with <3 % (Fig. 3A) and <5 % (Fig. 3B), respectively. Most likely, the high temperatures >850°C at UHP conditions (e.g. Schmädicke et al., 1992) led to higher MgO contents compared to FeO_{total} and higher TiO_2 contents in garnet, resulting in compositional overlap with garnet of mantle

origin for some grains. Besides these rare exceptions, both discrimination schemes clearly indicate a crustal origin of coesite- and diamond-bearing garnet grains; thus, fulfilling the definition of UHP metamorphism that refers to crustal rocks that experienced *P–T* conditions high enough for the formation of coesite (Carswell and Compagnoni, 2003).

[insert Figure 3, two-column fitting image]

3.2.2. Mafic versus felsic origin

Since a mantle origin is precluded (Section 3.2.1.), an important question to be answered is whether the coesite- and/or diamond-bearing garnet grains are sourced from metamorphic rocks of mafic or felsic bulk composition. The close association of mafic and metasedimentary UHP rock lenses and bodies within large volumes of medium- to high-pressure felsic country rocks is a common feature of UHP terranes, and often interpreted as mélanges of metamorphic rocks that do not share a joint *P–T* path (e.g. Liou et al., 2009). In contrast, a large and growing number of studies report findings of coesite and diamond in felsic country rocks of UHP terranes, which indicates subduction and exhumation as largely coherent geological units (e.g. Faryad and Cuthbert, 2020, and references therein). The felsic rocks often underwent strong retrogression or re-crystallization during exhumation that, based on the mineral assemblage, obliterates a precursor UHP stage (e.g. Hermann et al. 2006). Whether or not voluminous felsic rocks were involved in the cycle of UHP metamorphism has important implications for the size and buoyancy of UHP terranes to be considered in subduction and exhumation models (Zhang and Wang, 2020). Investigating the detrital record enables to systematically sample a mixture of lithologies that are potentially involved in the UHP rock cycle (including the felsic country rocks) and to screen those for inclusions of coesite and diamond preserved in resistant host minerals like garnet (Schönig et al., 2018a, 2019).

The scheme of Schönig et al. (2021a) facilitates the discrimination of garnet sourced from alkaline, calcsilicate, ultramafic, mafic, and intermediate–felsic/metasedimentary host-rock composition solely based on garnet major-element composition acquired by electron microprobe

analysis. As shown in Figure 4A, the scheme assigns a significant proportion of 45 % of the coesite- and diamond-bearing detrital garnets to an intermediate–felsic/metasedimentary source, with intermediate–felsic/metasedimentary host rocks predicted in all studied regions, except the two grains from the D'Entrecasteaux Islands of Papua New Guinea. Unfortunately, host-rock composition predictions for garnet from intermediate–felsic/metasedimentary eclogite-facies and UHP rocks are most challenging and show the highest misclassification rates with 50 % incorrectly assigned to a mafic source (see fig. 2 of Schönig et al., 2021a). Nevertheless, garnets from mafic eclogite-facies and UHP rocks are correctly assigned in 96 % of the cases and rarely misclassified as intermediate–felsic/metasedimentary. Thus, the 45 % of detrital UHP garnets assigned to an intermediate–felsic/metasedimentary source are rather a minimum estimation, clearly exceed misclassification rates, and indicate significant involvement of felsic rocks in the UHP rock cycle.

To gain further information about the source rocks of the garnets containing UHP mineral inclusions, a combination of detrital garnet chemistry and mineral inclusion assemblages has been shown to be of great value, particularly when compared to garnet of local crystalline rocks (Schönig et al., 2018a, 2018b, 2021b; Baldwin et al., 2021). This can be achieved by using garnet endmember plots or discrimination schemes (Wright, 1938; Morton, 1985; Teraoka et al. 1998; Schulze, 2003; Grütter et al., 2004; Mange and Morton, 2007; Aubrecht et al. 2009; Krippner et al., 2014; Hardman et al. 2018; Tolosana-Delgado et al., 2018; Schönig et al., 2021a).

[insert Figure 4, two-column fitting image]

Figure 4B (left diagram) shows a compositional comparison of detrital coesite-bearing garnet from Norway to garnet from local eclogite and felsic gneiss in the X_{Fe+Mn}–X_{Mg}–X_{Ca} ternary diagram. The coesite-bearing garnet grains show a considerable variability in X_{Ca}, indicating more than a single source. Based on the compositional similarity to garnet from local felsic gneiss, abundant inclusions of quartz, and the presence of an alkali feldspar inclusion, Schönig et al. (2018a) supposed a felsic source as most likely for coesite-bearing garnet showing the lowest X_{Ca} content (Fig. 4B, left). In contrast,

coesite-bearing garnet with the highest X_{Ca} content shows an inclusion assemblage of coesite + quartz + omphacite + kyanite + rutile, making a mafic source (i.e. eclogite) most likely.

The dataset of inclusion assemblages in detrital garnets from Germany studied by Schönig et al. (2019, 2020, 2021b) is much larger compared to that from Norway, and includes 2100 inclusion-bearing garnets (93 coesite-bearing, 54 diamond-bearing). This allows comparison of compositional characteristics of garnets containing specific inclusion types with garnet compositions from local crystalline rocks. Garnet grains hosting inclusions of omphacite and graphite have been found particularly useful. As shown in Figure 4B (middle diagram), the composition of omphacite-bearing garnet resembles the composition of garnet from local eclogites, whereas graphite-bearing garnet resembles the composition of garnet from local felsic rocks. Consequently, coesite- and diamond-bearing detrital garnets which additionally entrapped omphacite or which are compositionally similar to omphacite-bearing garnet are mainly sourced from mafic lithologies (eclogites), and those which additionally contain graphite or which are compositionally similar to graphite-bearing garnet are mainly sourced from felsic rocks. Based on a detailed comparison of detrital and crystalline garnet composition, as well as the consideration of other inclusion assemblages besides omphacite and graphite that are more common in felsic rocks (alkali feldspar, phlogopite–biotite, quartz, and cristobalite), Schönig et al. (2021b) assigned ~76 % of the coesite-bearing garnets to a felsic source and ~24 % to a mafic source. This highlights the importance of felsic lithologies in UHP rock cycles and indicates that the predicted proportion of detrital UHP garnet of felsic origin in Figure 4A (after Schönig et al., 2021a) represents a lower limit.

In addition to frequent hints that some UHP garnets are sourced from felsic lithologies, Schönig et al. (2020) observed that the composition of ~10 % of the coesite-bearing and ~7 % of the diamond-bearing grains only matches with garnet compositions from the felsic country rocks (yellow kernel density distribution map in Fig. 4B, middle diagram), which previously had been inferred not to have reached pressure conditions in excess of ~2.1 GPa (Willner et al., 1997; Tichomirowa et al., 2018). The main differences between this garnet and garnet from eclogite lenses (dark blue density distribution) as well as diamond-bearing felsic rock lenses (sky-blue density distribution) are the higher values of X_{Mn} and X_{Fe} versus X_{Mg} (Fig. 4B, middle diagram), which is becoming clear in scatter

plots of these ratios (see figs. 2 and 3 of Schönig et al., 2020). Thus, it was concluded that the felsic country rocks, diamond-bearing felsic lenses, and eclogites were subducted to UHP conditions as a largely coherent slab (Schönig et al., 2020). This supports individual opinions on the studied area (Gose and Schmädicke, 2018) as well as worldwide observations (Faryad and Cuthbert, 2020, and references therein), but strongly contradicts the view of a mixture of rocks that reached different maximum depth and amalgamated during exhumation (Massonne, 2005, 2011). Consequently, the interpretation based on detrital garnet data led to a relaunch of the debate about the geodynamic context of the UHP terrane of the central Saxonian Erzgebirge (Massonne, 2021; Schönig et al., 2021c).

Similar to the Erzgebirge of Germany, a comparison of detrital and crystalline garnet chemistry in the D'Entrecasteaux metamorphic complex of Papua New Guinea as well as inclusions of graphite and omphacite has proven useful. Only considering garnet composition, the coesite-bearing grains are assigned to a mafic source (Fig. 4A; after Schönig et al., 2021a). However, felsic UHP garnet is prone to be misclassified and Baldwin et al. (2021) suppose a felsic, probably metasedimentary, source based on a number of arguments.

First, detrital coesite-bearing garnet composition differs strongly from garnet of the coesite-bearing eclogite (Monteleone et al., 2007; Baldwin et al., 2008; Faryad et al., 2019; Osborne et al., 2019) (Fig. 4B, right diagram, purple density distribution). This observation is particularly important as the sample from the eclogite lens outcropping at a single location previously represented the only find of coesite in the UHP terrane of eastern Papua New Guinea, and thus the detrital coesite-bearing garnets significantly expand the range of lithologies involved in the UHP rock cycle (Baldwin et al., 2021).

Second, the two coesite-bearing garnets are compositionally distinct from garnet of other local eclogites as well as detrital garnet containing omphacite inclusions (Fig. 4B, right diagram, dark-blue and green density distributions), making a pristine eclogite source very unlikely. Furthermore, one of the coesite-bearing garnets contains abundant inclusions of graphite. As graphite is more likely to occur in metasedimentary rocks, and the composition of graphite-bearing detrital garnet resembles the composition of garnet from felsic rocks as well retrogressed eclogites and amphibolites (Fig. 4B, right

diagram, grey, yellow, and brown density distributions) but no inclusions of graphite have been found in garnet of a nearby retrogressed eclogite (see supplementary data 2 of Baldwin et al., 2021), a metasedimentary source is inferred to be most likely. Consequently, we interpret the detrital coesite-bearing garnets associated with this young, active UHP terrane to have formed from a protolith generated at Earth's surface, before subduction to and return from mantle depth, and subsequent erosion and deposition as a beach placer (Baldwin et al., 2021).

3.3. Methodological benefits and limits

Almost all previous studies dealing with UHP metamorphism are based on analyzing crystalline rocks, whereby potential rocks are sampled following targeted field mapping. When the aim is to examine the existence and/or extent of UHP rocks this approach suffers in some respects, particularly when large rock volumes have to be screened (Schönig et al., 2018a).

First of all, crystalline rocks commonly outcrop poorly or are not accessible in the area of interest. Depending on climate conditions and lithology, bedrocks may be covered by soil, dense vegetation, or ice. Even if a large area may be well exposed and lithologies have been comprehensively mapped, the selection of sampling spots might be challenging and sometimes subjective regarding the large volumes of rocks. Equilibration under UHP metamorphic conditions may depend on fluid infiltration, which can result in co-existing domains of different metamorphic grade on very small scales (e.g. John and Schenk, 2003). To make matters worse, UHP terranes are commonly exhumed by nearly isothermal decompression or even heating before cooling and thus metamorphic peak assemblages usually are not preserved and/or obliterated by retrogression (e.g. Ernst, 2006). Particularly felsic rocks are prone to be retrogressed due to melting induced by the breakdown of hydrous phases like phengite (Hermann et al, 2006). UHP minerals like coesite and diamond may survive retrogression when shielded from the external conditions by their entrapment as inclusions in resistant host minerals like garnet; however, this is difficult to assess during sampling in the field. In contrast, analyzing detrital grains takes advantage of natural processes such as erosion and sedimentary transport to sample potential host minerals from a variety of rocks in the investigated

catchment (e.g. Schönig et al., 2018a). This also includes grains from rocks which have undergone weathering, soil formation and/or are covered by vegetation or ice (sampled by meltwater).

A tremendous advantage is the possibility to apply the method to ancient clastic sedimentary rocks (e.g. Schönig et al., 2018a; Baldwin et al., 2021). Because garnet (i) represents a common detrital mineral in sediments originating from orogenic settings (e.g. Andò et al., 2014), (ii) can preserve UHP mineral inclusions (e.g. Schönig et al. 2018a, 2019) even when exhumed under high-temperature conditions (Schönig et al., 2020; Baldwin et al., 2021), and (iii) is comparatively stable during transport, surface weathering, and deep burial (Morton and Hallsworth, 1999), it can be expected that coesite- and/or diamond-bearing garnets are preserved in ancient sedimentary successions shed from UHP terranes, like already shown for coesite-bearing zircon (Chen et al., 2005). Thus, garnet is a major target mineral to study the erosion and exposure of ancient UHP terranes with high potential regarding, for instance, dimensions of rock bodies affected by UHP conditions, timing and rates of UHP rock exhumation to Earth's surface, as well as the occurrence of UHP terranes throughout Earth's history. However, the preservation in ancient sedimentary rocks still has to be tested and validated.

Although the detection of UHP sources by analyzing detrital minerals offers several benefits, it is also accompanied by some challenges. First and foremost, some powerful techniques of metamorphic petrology cannot be applied directly. Metamorphic thermobarometry is based on exchange reactions, exsolution temperature of solid solutions, net-transfer reactions, major-element contents, trace-element partitioning, multi-equilibria calculations, petrogenetic grids, and thermodynamic modelling. All these methods can provide detailed information on *P–T* evolution but most of them depend on two or more co-existing minerals and/or knowledge of the (effective) bulk-rock composition (e.g. Reverdatto et al., 2019). Because this information is highly limited concerning detrital single grains, detailed *P–T* information is not available and can only roughly be estimated by using garnet discrimination schemes and combine the results with inclusion information (Section 3.2.) or by applying elastic thermobarometry (Baldwin et al., 2021). Nevertheless, the method of analyzing inclusions in detrital garnet provides a first-order overview of the distribution and characteristics of UHP metamorphic rocks located in the study area, and thus can be seen as an effective starting point

to plan further exploration – or not. It is capable of verifying the presence of UHP rocks and providing source rock characteristics, as long as the eventuality of a mantle origin is carefully considered (Section 3.2.1.).

Analyzing detrital grains requires considering the eventuality of sediment recycling. Although detrital garnet containing coesite and/or diamond inclusions provides evidence for material of UHP origin located in the present-day catchment, it is uncertain whether the UHP garnets originated directly from crystalline rocks or, if present, may be reworked from sediments or sedimentary rocks within the catchment. This is a difficulty, but remains a minor problem if the catchment area is relatively small, clearly arranged, and geologically well known. However, it becomes tricky for large catchments, remote areas, and when analyzing sedimentary rocks with unknown origin. Thus, tackling the recycling issue strongly depends on the respective geological situation and the objectives of the study.

One of the key objectives is to link detrital coesite- and/or diamond-bearing garnet to a specific metamorphic/orogenic event. In this case, dating zircon, monazite, rutile, and/or apatite grains from the bulk sediment sample will reveal whether more than a single event or an exotic input has to be considered. If not, sediment recycling with respect to UHP minerals can be neglected. If yes, direct *in-situ* dating of the host mineral containing UHP inclusions is the method of choice. Unfortunately, aluminum-rich garnet is typically poor in uranium, hampering the ability of U–Pb dating. However, first successful approaches of dating uranium-poor aluminum-rich garnet in the U–Pb system (Millonig et al., 2020) and the Sm–Nd system (Maneiro et al., 2019) are encouraging. Other suitable dating techniques strongly depend on mineral inclusions co-existing with the UHP phases and have to be adjusted to the specific case. For instance, (U, Th)–Pb dating of monazite (e.g. Harrison et al., 1997; Martin et al., 2007), zircon (e.g. Usui et al., 2002; Bruguier et al., 2017), or rutile inclusions (e.g. Bruguier et al., 2017; Zhou et al., 2020) in close proximity to UHP inclusions would be a possibility. In addition, expanding the technique to other host minerals that can be confidently dated in the U–Pb system, like zircon and rutile, would certainly increase the precision in age determinations.

If contamination from sediments in the catchment cannot be excluded and dating is not feasible or data remains ambiguous, the information provided by the detrital garnets is still very useful to

quickly narrow down the potential source rocks by comparing their chemical characteristics and inclusion assemblages with that of garnet from local crystalline rocks located in the catchment.

3.4. Enhancing efficiencies

It has been shown, for three different UHP terranes of different age and with continental as well as oceanic upper plates, that analyzing detrital garnet grains is effective in identifying UHP metamorphic rocks and less time consuming than analyzing many crystalline rock samples from large volumes of potential UHP lithologies. However, the user-assisted time needed for analyzing mineral inclusion assemblages in a large number of detrital garnet grains by Raman spectroscopy is still extensive. Enhancing efficiencies of the method becomes particularly important when considering (i) prospective applications to large regions where many samples from large drainage systems shall be screened for the presence of coesite- and diamond-bearing garnet or (ii) ancient sedimentary rocks where catchment size and complexity regarding bedrock geology are often arguable. Techniques that enable a statistically based pre-selection of potential UHP garnet grains seems most promising to reduce the overall analytical time, while automated measurement routines are most promising to reduce the user-assisted time.

3.4.1. Selecting the grain-size window

The analyzed grain size can have a strong control on the composition (Krippner et al., 2015; Krippner et al., 2016; Schönig et al., 2021b) and mineral inclusion assemblages of detrital garnet (Schönig et al., 2018b, 2021b). On the one hand, variations in composition and inclusions leads to variations in garnet density, which in turn affects the hydrodynamic behavior. However, stronger control has been observed regarding the initial garnet crystal size at the source, that varies markedly between different garnet-bearing rocks and is prone to be inherited in their erosional material, i.e. sediments (Krippner et al., 2015; Krippner et al., 2016; Schönig et al., 2021b). This raises the question whether garnet sourced from UHP rocks is enriched in a specific grain-size window, and thus whether a pre-selection of the grain-size window can enhance analytical efficiencies.

The grain-size distribution of coesite- and diamond-bearing detrital garnet from the Saxonian Erzgebirge has been studied in detail by Schönig et al. (2021b). Reports of garnet composition for different grain-size windows indicate that garnet sourced from high-grade metamorphic rocks is often enriched in the medium-sand fraction compared to fine-sand (see fig. 1 of Schönig et al., 2021b). While diamond-bearing garnet follows this trend, the grain-size distribution of coesite-bearing garnet is highly heterogenous. It turned out that this effect comes along with variations in source-rock composition. UHP garnet shed from mafic rocks contains a low number of coesite inclusions and is typically enriched in coarser grain-size fractions due to grain-size inheritance. In contrast, UHP garnet derived from felsic rocks contains variable amounts of coesite inclusions, whereby coesite-poor grains are enriched in coarser fractions (similar to mafic UHP garnet), but coesite-rich grains are enriched in fine fractions. Due to different elastic properties of coesite and garnet, strains developing during exhumation cause a high degree of fracturing and fracture connections to smaller inclusions for coesite-rich grains, allowing fluid infiltration and the transformation to quartz, which in turn further promotes garnet disintegration (see figs. 13 and 14 of Schönig et al., 2021b).

In order to figure out the most efficient grain-size fraction for tracing UHP metamorphism, Schönig et al. (2021b) relate the frequency of coesite- and diamond-bearing garnet in different grain-size fractions to the analytical time needed, which increases with increasing garnet grain size. Due to the heterogenous grain-size distribution of coesite-bearing garnet, the most efficient grain-size fraction varies between catchments that comprise varying proportions of mafic and felsic host rocks. On average, none of the grain-size fractions was found to be more efficient compared to any other with regard to the number of UHP garnets detected per time (see fig. SM5 of Schönig et al., 2021b), and thus the fraction that provides the highest value of information should be defined as most efficient. Solely the 250–500 µm fraction recorded (i) UHP metamorphism in all studied catchments, (ii) coesite-bearing garnet from mafic as well as felsic sources for individual catchments, and (iii) diamond-bearing garnet in the respective catchments (Schönig et al., 2021b). This also holds for detrital garnet from Papua New Guinea, where coesite-bearing garnet has only been detected in the >200 µm fraction (Baldwin et al., 2021). In contrast, detrital coesite-bearing garnet from Norway is absent in the 250–500 µm but most abundant in the 63–125 µm fraction (Schönig et al., 2018a). In

conclusion, to reduce the analytical time in order to screen large rock volumes by a large number of samples on the occurrence of UHP rocks, the 250–500 µm grain-size fraction is most efficient for initial analysis. This cannot be generalized and an absence of UHP garnet in this fraction does not exclusively rule out their existence, but makes it much less likely in particular on a statistical base by considering multiple samples (Schönig et al., 2021b).

3.4.2. Geochemical pre-screening

Garnet major-element composition is mainly a function of pressure, temperature, effective bulk-rock composition, and fluid availability. As information about the bulk-rock composition is very limited from a detrital perspective, multivariate quantitative empirical approaches applied to large natural datasets are most promising to estimate the metamorphic grade of garnet formation solely based on garnet major-element composition (Tolosana-Delgado et al., 2018; Schönig et al., 2021a). These discrimination schemes may allow screening out of garnet grains that are less likely to have crystallized during UHP metamorphism, and thus reduce the number of grains selected for the time-consuming inclusion analysis.

The discrimination scheme of Tolosana-Delgado et al. (2018) rests on a model developed by applying linear discriminant analysis to a major-element dataset of 3,188 garnets. As a result, it assigns garnet grains with specific probabilities to five major host-rock types, that are (i) ultramafic rocks, (ii) felsic igneous rocks, (iii) amphibolite-facies metamorphic rocks, (iv) granulite-facies metamorphic rocks, and (v) eclogite-facies metamorphic rocks. Notably, the scheme does not differentiate between eclogite-facies garnet of crustal and mantle affinity. Thus, a mantle origin should be additionally considered by applying the scheme of Hardman et al. (2018) or Schönig et al. (2021a) (Section 3.2.1.).

Considering the arithmetic mean probabilities of individual detrital coesite- and diamond-bearing garnet grains analyzed at 9–20 spots per grain, the scheme of Tolosana-Delgado et al. (2018) assigns all grains to a metamorphic source (using the prior probability ‘equal-M’). Figure 5A shows the probabilities of the individual grains for the three considered metamorphic rock types. The scheme assigns ~81 % of the grains with the highest probability of belonging to an eclogite-facies

metamorphic source. This rate slightly decreases to ~79 % or ~78 % when additionally sorting out grains that are assigned to a mantle origin based on the schemes of Hardman et al. (2018) or Schönig et al. (2021a), respectively (Fig. 3).

[insert Figure 5, two-column fitting image]

The discrimination scheme of Schönig et al. (2021a) is based on a model trained on a major-element dataset of 13,615 garnets using the random forest machine-learning algorithm. The "setting and metamorphic facies" model consists of an ensemble of 3,400 deeply grown classification trees. For a specific garnet composition, each tree votes for one of seven host-rock classes, that are (i) mantle rocks, (ii) metasomatic rocks, (iii) igneous rocks, (iv) blueschist-/greenschist-facies metamorphic rocks, (v) amphibolite-facies metamorphic rocks, (vi) granulite-facies metamorphic rocks, and (vii) eclogite-facies/ultrahigh-pressure metamorphic rocks. Garnet grains are assigned to the class that receives the majority of the votes from the 3,400 trees.

Considering the arithmetic mean votes of 9–20 spots per grain after Schönig et al. (2021a), none of the detrital coesite- and diamond-bearing garnet grains is assigned to an igneous or metasomatic origin, but <3 % received a higher number of votes for a mantle origin than the maximum of votes for the four metamorphic classes (Fig. 3B). Figure 5B shows the individual votes for the metamorphic classes for garnet grains that are assigned to a metamorphic origin in Figure 3B. The scheme assigns the majority of votes to metamorphic garnet of the eclogite-facies/ultrahigh-pressure class for ~87 % of the coesite- and diamond-bearing grains, and thus provides a higher success rate compared to Tolosana-Delgado et al. (2018; Figure 5A) and a more efficient pre-screening.

By using the arithmetic mean probabilities or votes for the single grains in the two tested schemes, the eventuality of major-element zonation is ignored. Strong zonation of detrital garnet derived from regional metamorphic rocks is rather scarce, and can lead to misclassification (Krippner et al., 2014). To estimate the impact of zonation and/or compositional intra-grain variability, Figure 6 shows the discrimination results of all individual analyses (9–20 spots per grain) for coesite- and diamond-bearing garnet grains that have not been classified as being sourced from eclogite-facies

rocks by mean probabilities after Tolosana-Delgado et al. (2018) and mean votes after Schönig et al. (2021a) (cf. Fig. 5). In both schemes, most analyses are still classified as granulite- or amphibolite-facies garnet, but ~15 % and ~7 % are assigned to the eclogite facies, respectively (Fig. 6). Transferring this to the number of grains, this corresponds to an increase in UHP garnet assigned to the class of eclogite-facies garnet from 81 to 90 % for the scheme of Tolosana-Delgado et al. (2018) and from 87 to 92 % for the scheme of Schönig et al. (2021a). However, this increase in success is laborious as the number of electron microprobe analyses considered has been increased from 155 to 1,439, that is by >800 %. Consequently, although zonation and/or compositional intragrain variability is an issue, it is more efficient from a statistical perspective to pre-screen a larger number of grains by one spot and accept that some UHP grains may be sorted out than pre-screening a smaller number of grains by multiple spots.

[insert Figure 6, two-column fitting image]

Such a geochemical pre-screening technique becomes particularly powerful for large catchments that drain a variety of potential garnet source rocks. A striking example is sample JS-Erz-14s of Schönig et al. (2019, 2020). This modern sand sample represents erosional material from a regional river catchment that drains an area >500 km^2, comprising the UHP terrane of the central Saxonian Erzgebirge as well as the surrounding nappes of lower metamorphic grade. A total of 300 inclusion-bearing garnet grains have been investigated regarding inclusion assemblages, comprising 100 grains from each, the 63–125 µm, 125–250 µm, and 250–500 µm grain-size fraction. Coesite inclusions occur in six of the grains, two from the 125–250 µm fraction and four from the 250–500 µm fraction. In addition, one diamond-bearing garnet has been found in the 250–500 µm fraction. Figure 7 shows the discrimination results of all inclusion-bearing garnets in the ‘setting and metamorphic facies’ scheme after Schönig et al. (2021a). Grains that contain UHP mineral inclusions (coesite or diamond) and grains that do not contain UHP inclusions are marked individually for the different grain-size fractions. Votes in the ‘setting’ plot (Fig. 7, upper diagram) assign the majority of garnets (96 %) to a metamorphic source. For these garnets, individual votes for the four metamorphic-facies

classes are shown in the ‘metamorphic facies’ plot (Fig. 7, middle diagram). Considering a pre-screening where all garnet grains that are not assigned to the eclogite/ultrahigh-pressure class are sorted out, ~56 % of all grains are excluded prior to inclusion analysis (Fig. 7, lower diagram), being accompanied by a considerable saving of analytical time. Thereby, all UHP garnets from the 125–250 µm as well as 80 % of the 250–500 µm fraction are maintained. The rate is even more impressive when the grain-size fraction with the most potential (250–500 µm; Section 3.4.1.) is considered individually, where ~78 % of the grains are sorted out by maintaining 80 % of the UHP garnets.

[insert Figure 7, single-column fitting image]

3.4.3. Hyperspectral three-dimensional Raman imaging

Analyzing inclusions in a large number of detrital mineral grains by manually focusing on the individual inclusions is a time-consuming procedure (Schönig et al., 2021b). In addition, to run labs efficiently, techniques that enable automatic acquisition of data beyond user active hours are highly welcome. Raman imaging by largely automated systems provide this option. Figure 8 shows a hyperspectral cuboid acquired from a 70 × 60 × 20 µm garnet volume at three different resolutions.

[insert Figure 8, two-column fitting image]

Analysis was performed at the Geosciences Center Göttingen, Germany. The experimental setup includes a WITec alpha 300R fiber-coupled ultra-high throughput Raman spectrometer, a 532 nm laser, an automatically adjusted laser power of 20 mW, a 300 l×mm^{-1} grating, a 100× long working distance objective with a numerical aperture of 0.75, an acquisition time of 20 ms per spectrum, and an electron multiplying charge-coupled device. The cuboid with the highest resolution (step size of 0.25 × 0.25 × 0.25 µm) offers many details, including the thin rim of quartz in the largest inclusion and the detection of a very small coesite inclusion with a size of <2 µm. However, the total duration of the experiment of >40 hours is inefficient for the objective of detecting and identifying inclusion in a large number of garnets. By adjusting the step size to 1.00 × 1.00 × 1.00 µm, the

smallest inclusion is not detected but all other inclusions as well as the bimineralic character of the largest are detected. This also holds for a step size of 2.00 × 2.00 × 2.00 µm, whereby the total duration is only ~7 min. This setup was tested on several detrital garnet grains from the Saxonian Erzgebirge, revealing that most mineral inclusions ≥4 µm are confidently identified. Smaller inclusions ≤3 µm are identified for strong Raman active phases like coesite, quartz, diamond, and rutile. For the coesite-bearing garnet grains from the Erzgebirge, 84 of the 93 garnets (~90 %) have at least one coesite inclusion ≥3 µm. Thus, hyperspectral Raman imaging offers a great option to reduce the user-assisted analytical time needed for inclusion analysis.

4. Other potential UHP host minerals

Besides garnet, coesite and diamond inclusions have been frequently detected in other host minerals like zircon (e.g. Parkinson and Katayama, 1999; Massonne, 2003), clinopyroxene (e.g. Smith, 1984; Shatsky and Sobolev, 1993), and chromite (e.g. Robinson et al., 2004; Yamamoto et al., 2009). In addition, they were also found in tourmaline (e.g. Ota et al., 2008; Marschall et al., 2009), rutile (e.g. Hart et al., 2016; Rezvukhina et al., 2021), kyanite (e.g. Massonne, 2003; Taguchi et al., 2019), titanite (Ogasawara et al., 2002), zoisite (Shatsky and Sobolev, 1993), epidote (Zhang et al., 1995), and dolomite (Zhang and Liou, 1996).

For the sedimentary record of UHP metamorphism, the so-called ultrastable minerals are of particular importance, namely zircon, rutile, and tourmaline. These are common in high-grade metamorphic rocks, and due to their extreme stability against mechanical abrasion and chemical weathering, they are also common phases in mature clastic sediments and sedimentary rocks (e.g. Hubert, 1962). Additionally, they survive in deeply buried sedimentary successions (>3000 m), at depths were garnet (especially grossular-rich garnet) may break down by intrastratal solution (e.g. Morton and Hallsworth, 1999). Thus, these ultrastable minerals have high potential to archive UHP metamorphism in the sedimentary record.

4.1. Zircon

In addition to the possibility of screening very mature sediments on the presence of erosional material sourced from UHP rocks, a major advantage of finding UHP inclusion in detrital zircon is the straightforward application of geo- and thermochronometric methods. The low contents of non-radiogenic lead and the high closure temperature of >900 °C (Dahl, 1997) make zircon the most commonly utilized mineral for determining crystallization ages (e.g. Corfu et al., 2003). This is nowadays routinely performed by, for instance, laser ablation inductively coupled plasma mass spectroscopy (e.g. Frei and Gerdes, 2009) or secondary ion mass spectroscopy (e.g. Ireland and Williams, 2003). Furthermore, simultaneous analysis of rare-earth-element (REE) concentrations enables to discriminate mantle and crustal zircon. Compared to crustal zircon, zircon from mantle rocks shows low REE concentrations, a flat REE pattern, and low thorium and uranium contents (Belousova et al., 1998, 2002; Hoskin and Ireland, 2000). Combining those high-spatial-resolution techniques with cathodoluminescence and/or back-scattered-electron imaging enables to directly link a growth zone of a detrital zircon that contains coesite and/or diamond to a specific metamorphic event that includes deep subduction of continental crust (Wan et al., 2005). Notably, caution must be taken to rule out a secondary origin of UHP mineral inclusions (pseudo-inclusions) as demonstrated by coesite inclusions found in magmatic zircon that were introduced during UHP metamorphism via cracks that provide fluid pathways (Gebauer et al., 1997; Zhang et al., 2009; Schertl et al., 2019). In addition, diamond abrasives should not be used during sample preparation to avoid contamination-related misinterpretations (Dobrzhinetskaya et al., 2014).

Besides the determination of UHP crystallization ages, thermochronological methods can be applied, that is the determination of cooling ages by zircon fission track (e.g. Kohn et al., 2019) or (U-Th)/He dating (e.g. Reiners, 2005). Both methods may be combined with U–Pb crystallization ages derived from the same grain (Carter and Moss, 1999; Rahl et al., 2003; Reiners et al., 2004, 2005; Campbell et al., 2005; Bernet et al., 2006; McInnes et al., 2009; Evans et al., 2013), enabling estimation of exhumation rates (e.g. Enkelmann et al., 2008; Wang et al., 2014). In addition, the titanium content in zircon mainly depends on temperature and to lesser extent on pressure, allowing estimation of crystallization temperatures (Watson and Harrison, 2005; Watson et al., 2006; Ferry and Watson, 2007).

Despite the wealth of information provided by zircon, the applicability of using inclusions in zircon to trace the erosion of UHP rocks is hampered by the strong dilution of high-grade metamorphic zircon in the sediment factory. First of all, most zircon is formed in intermediate–felsic igneous rocks, and thus igneous zircon dominates the detrital record (e.g. Balica et al., 2020). Secondly, the timing of zircon growth in metamorphic systems is a further aggravating factor. Zirconium mass balancing models indicate that zircon in equilibrium with co-existing mineral phases primary dissolves on the prograde metamorphic path and mainly grows during exhumation and cooling, thus often postdates peak-pressure conditions (Kohn et al., 2015). However, prograde growth of zircon from fluids is facilitated by dehydration reactions (e.g. Gauthiez-Putallaz et al., 2016). In addition, dissolution of inherited zircon and formation of new metamorphic zircon from released zirconium (dissolution–precipitation process) enables prograde zircon growth in a virtually closed system without the need of significant amounts of free fluids with high zirconium solubility (e.g. Tomaschek et al., 2003; Rubatto et al., 2008). Inclusions of coesite and/or diamond in zircon of the Kokchetav massif (e.g. Parkinson and Katayama, 1999; Hermann et al., 2001), the Saxonian Erzgebirge (Massonne, 2003; Massonne et al., 2007), and the Qinling–Dabie–Sulu Orogen (e.g. Parkinson and Katayama, 1999; Ye et al., 2000; Liu et al., 2008) demonstrate the growth of zircon at UHP conditions, and the preservation of those zircons in the sedimentary record (Chen et al., 2005). Thus, from a detrital perspective, finding an efficient pre-screening technique to get rid of the overwhelming amount of igneous and low-pressure metamorphic zircon poses the major challenge.

To discriminate magmatic from metamorphic zircon, considering the zoning pattern and the ratio of thorium-to-uranium are simple and powerful tools. The majority of magmatic zircon shows oscillatory zoning and thorium-to-uranium values >0.1, while metamorphic zircons show values <0.1 (Rubatto and Gebauer, 2000; Belousova et al., 2002; Rubatto, 2002; Grimes et al., 2015). Notably, this threshold should be used with caution (Harley et al., 2007; Rubatto, 2017; Yakymchuk et al., 2018), as several cases of metamorphic zircon with higher thorium-to-uranium ratios have been reported (Pidgeon, 1992; Vavra et al., 1996, 1999; Carson et al., 2002; Möller et al., 2002, 2003; Hokada and Harley, 2004; Kelly and Harley, 2005; Ewing et al., 2013; Korhonen et al., 2013; Stepanov et al., 2016). However, a compilation by Rubatto (2017) shows that by far the most UHP zircons have a

thorium-to-uranium ratio <0.2, and higher values are restricted to rare cases of ultrahigh-temperatures (UHT) at UHP conditions (Stepanov et al., 2016). This is related to the high solubility of monazite in melts produced at UHT metamorphic conditions (Stepanov et al., 2012, 2014), leading to thorium enrichment in zircon crystallized from the UHT melt (Rubatto, 2017).

In addition to the thorium-to-uranium ratio, REE patterns are potentially useful to identify HP/UHP metamorphic zircon. First, HP/UHP zircon primary crystallizes in the presence of garnet. As garnet preferentially incorporates heavy REEs (HREE), co-genetic zircon is characterized by a flat HREE pattern (e.g. Rubatto, 2002, 2017, and references therein). Notably, a similar pattern can also be produced by abundant co-existing orthopyroxene that is able to incorporate high amounts of HREE (Fornelli et al., 2014). Second, albite – a main carrier of europium – breaks down in the HP blueschist and eclogite facies to form quartz and jadeite (Holland, 1980), leaving an europium-enriched effective bulk-rock composition. Thus, zircon crystallized at eclogite-facies condition is often characterized by a weak or absent negative europium anomaly (e.g. Rubatto, 2002; Baldwin et al., 2004), but exceptions exist for bulk-rock compositions with very strong depletion in europium or enrichment in HREE (Rubatto, 2017, and references therein). It is important to mention that deeply crystallized magmatic zircon also shows a less pronounced negative europium anomaly due to the decreasing stability of plagioclase and increasing stability of garnet and amphibole (Tang et al., 2021a). This observation has been used to infer crustal thickness through time on a regional and global scale (Tang et al. 2021a, 2021b).

In summary, a statistically-based pre-selection scheme to enrich the strongly diluted detrital zircons sourced from HP/UHP metamorphic rocks should consider a combination of indicators. Particularly, an absence of oscillatory zoning, a low thorium-to-uranium ratio, a flat HREE pattern, and a weak or absent negative europium anomaly constitutes a high probability of facing zircon of HP/UHP origin.

4.2. Rutile

In contrast to zircon, rutile growth is more common in HP metamorphic rocks and less common in mantle rocks, igneous rocks, hydrothermal systems (e.g. Force, 1980; Zack and Kooijman, 2017). Consequently, rutile of high-pressure metamorphic origin is inherently enriched in the sediment factory and rutile growth at UHP conditions is confirmed by reports of coesite (Hart et al., 2016) and diamond inclusions (Massonne, 2003; Rezvukhina et al., 2021). Furthermore, the chemical composition of rutile enables to discriminate (i) mantle rutile by higher aluminum and magnesium contents (Smythe et al., 2008) as well as higher zirconium to hafnium ratios (Pereira et al., 2019) compared to crustal rutile, and (ii) igneous and hydrothermal rutile from metamorphic rutile by concentrations and ratios of niobium, tantalum, zirconium, hafnium, tungsten, antimony, zinc, vanadium, chromium, and iron (Clark and Williams-Jones, 2004; Agangi et al., 2019; Pereira et al., 2019).

A tremendous advantage of considering rutile as detrital UHP recorder is the possibility to date the specific metamorphic event in the U–Pb system even when zircon growth at UHP conditions was lacking. While zircon may miss specific metamorphic stages (Thiessen et al., 2019) or even entire tectonothermal events (Moecher and Samson, 2006; Krippner and Bahlburg, 2013), rutile typically records the last orogenic event (von Eynatten and Dunkl, 2012, and references therein). This is because rutile is prone to break down and form low-pressure titanium-rich phases like titanite, ilmenite, or biotite during subsequent metamorphic cycles even at greenschist-facies conditions (Zack et al., 2004a; Luvizotto et al., 2009; Luvizotto and Zack, 2009; Meinhold, 2010; Triebold et al., 2012). In comparison to zircon, important to note is the much lower U–Pb closure temperature of 400–600 °C (Vry and Baker, 2006; Kooijman et al., 2010; Blackburn et al., 2011; Zack et al., 2011). Thus, rutile U–Pb ages primarily reflect cooling ages of UHP rocks, except for extremely low geothermal gradients.

In addition, finding coesite or diamond inclusions in detrital rutile is particularly attractive to enhance information about the UHP source rocks. Niobium versus chromium contents are useful for discriminating mafic versus felsic sources (Zack et al., 2004a; Triebold et al., 2007; Meinhold et al., 2008; Triebold et al., 2012), whereby a felsic source can further be supported by a large spread and on average elevated Hf concentrations (Meinhold, 2010). Rutile further serves as a thermometer, due to

the temperature-dependent partitioning of zirconium when co-existing with zircon and quartz (Zack et al., 2004b; Watson et al., 2006; Tomkins et al., 2007, Kohn, 2020). Notably, niobium versus chromium host-rock classification and zirconium-in-rutile thermometry are not always valid for temperatures >900°C (Kooijman et al., 2012; Hart et al., 2018, and references therein).

Challenging factors for analyzing mineral inclusions is the intrinsic color of rutile (less transparent than garnet and zircon) and the intense Raman activity. This hampers the optical inclusion detection and obscures the Raman signal emitted by the inclusions. Thus, analytical techniques probably have to be customized, for example by grinding/polishing in several steps and/or by significantly reducing the analyzed volume by using shorter laser wavelength and higher numerical apertures. Regardless of this minor shortcoming to be tackled, rutile has a high potential for detrital UHP studies with regard to source rock chronology, thermometry, and composition.

4.3. Tourmaline

Tourmaline is a common mineral in metasedimentary rocks, but is even more common in felsic igneous rocks (e.g. Henry and Guidotti, 1985; von Eynatten and Dunkl, 2012). Although scarce, tourmaline growth at UHP conditions is indicated by quartz pseudomorphs after coesite in tourmaline of the Dora Maira Massif in the Western Alps (Ertl et al., 2010) and coesite-bearing tourmaline from Lago di Cignana in the Western Alps (Reinecke, 1991; Bebout and Nakamura, 2003) and the Saxonian Erzgebirge in the Northeastern Bohemian Massif (Marschall et al., 2009). In addition, diamond-bearing tourmaline is reported from the Kokchetav Massif in Kazakhstan, although tourmaline growth in the diamond stability field is uncertain (Ota et al., 2008).

Major element chemistry is useful to discriminate metamorphic from igneous tourmaline. Metamorphic tourmaline shows high proportions of Mg compared igneous tourmaline, and igneous tourmaline additionally has high concentrations of Al, Fe, and Li (Henry and Guidotti, 1985; von Eynatten and Gaupp, 1999; Morton et al., 2005; Trumbull et al., 2009). In addition, boron isotopes can provide valuable source rock information (Guo et al., 2021). The high closure temperature in isotopic systems like K–Ar, ^{40}Ar–^{39}Ar, Rb–Sr, Sm–Nd, and U–Th–Pb also provide the opportunity for

geochronological dating of tourmaline (Marschall and Jiang, 2011), although this has not been utilized much yet (e.g. Martínez-Martínez et al., 2010).

5. Fields of application

5.1. Exhumation history of UHP terranes

Sedimentary provenance analysis commonly aims at reconstructing the exhumation history of orogens in the hinterland by investigating sedimentary successions of foreland basins. As a major advantage, the timing of exhumation and sometimes even rates may be constrained by stratigraphic means. However, identifying the metamorphic grade of eroded source rocks is challenging because most grains lost their paragenetic context. Thus, unless gravel-sized material is available, diagnostic associations of minerals in mutual grain contact, i.e. metamorphic mineral assemblages, cannot be observed and information must be extracted from detrital single grains (von Eynatten and Dunkl, 2012).

While a distinct change in the heavy mineral assemblage may mark the onset of metamorphic input into a basin, for instance by the first significant appearance of metamorphic minerals like epidote, garnet, and/or hornblende, the exposure of HP and UHP units in the hinterland is often difficult to assess, especially in mature sedimentary successions. Diagnostic index minerals, like omphacite, glaucophane, and lawsonite for HP metamorphism or coesite and diamond for UHP metamorphism, are rarely archived in the sedimentary record. Often these minerals are either replaced by low-pressure phases during exhumation of their initial source rocks, or, when preserved and exposed to the surface, they progressively disappear when subjected to processes of the sedimentary cycle such as weathering and transport. Therefore, in most cases single-grain techniques like the determination of the Si content in white mica (e.g. von Eynatten et al., 1996; Grimmer et al., 2003), garnet chemistry (e.g. Morton, 1985; Krippner et al., 2016), rutile chemistry (e.g. Triebold et al., 2007; Meinhold et al., 2008) or the comparison of chronological data with known ages from potential source rocks (e.g. Li et al., 2005; Weislogel et al., 2006) are applied to detect the exposure and erosion of high-grade metamorphic rocks. Although these methods are generally suitable to evaluate the

exhumation history of crystalline rock packages, detailed information on exhumation stage and metamorphic grade of exposed rocks is open for interpretation.

In contrast, by applying the concept of analyzing inclusions in mechanically and chemically stable host minerals, the first supply of material sourced from HP/UHP metamorphic rocks can be pinpointed, even in mature sediments. The host mineral shields inclusions from retrogression and modifications during surface weathering, transport, and burial diagenesis. Inclusions of omphacite in garnet directly reflect an eclogitic source and thus the exposure and erosion of HP rocks in the source area (Schönig et al., 2018b). Although not reported from the detritus so far, inclusions of glaucophane or lawsonite would reflect low-temperature HP source rocks. Continued exhumation and exposure of UHP rocks can be verified by inclusions of coesite and, at higher pressures, diamond (Schönig et al., 2018a, 2019, 2020; Baldwin et al., 2021). This opens new opportunities to investigate the timing of exposure of HP and UHP rocks, respectively, and trace the exhumation history, for example by estimating the exhumation rates of ancient HP/UHP terranes.

5.2. Modern-style plate tectonics in Earth history

Plate tectonics is a unique feature of planet Earth (e.g. Stern, 2018; Dewey et al., 2021), driven by the global-scale operation of subduction, i.e., the sinking of cold dense lithosphere into the mantle (Forsyth and Ueda, 1975; Conrad and Lithgow-Bertelloni, 2002). Thus, the time interval where subduction started to exert a dominant control on continental crust generation and preservation marks the onset of plate tectonics (e.g. Dhuime et al., 2012; Hawkesworth et al., 2016), whereby the transition from local- to global-scale subduction might have been a long-term process (Bercovici and Ricard, 2014). Several lines of arguments, like the first appearance of paired metamorphic belts (Brown, 2006, 2014), the formation of large continental masses (e.g. Korenaga, 2013; Hawkesworth et al., 2016; Reimink et al., 2021), the decrease in the rate of continental growth (e.g. Belousova et al., 2010; Dhuime et al., 2012, 2015, 2017; Spencer et al., 2017), geochemical data (Cawood et al., 2006; Shirey and Richardson, 2011; Tang et al. 2016; Satkoski et al., 2017), and petrological-thermomechanical numerical modelling (Sizova et al., 2010) indicate an onset of subduction in the Mesoarchean to early Paleoproterozoic (e.g. Brown et al., 2020; Palin et al., 2020). In contrast, some

authors argue for an even earlier onset of subduction during late Hadean to early Archean times (e.g. Komiya et al., 1999; Nutman et al., 2002, 2020; Hopkins et al., 2008, 2010; Pease et al., 2008; Shirey et al., 2008; Ernst, 2017; Greber et al., 2017; Maruyama et al., 2018), and others argue for an onset as late as the Neoproterozoic (Stern, 2005; Hamilton, 2011; Stern et al., 2016).

While Hadean to early Archean plate tectonic phenomena may be related to local subduction in an otherwise global stagnant-lid regime (Toth and Gurnis, 1998; Gurnis et al., 2004; Ueda et al., 2008; Burov and Cloetingh, 2010; Gerya et al., 2015; Davaille et al., 2017; O'Neill et al., 2018; Brown et al., 2020), the key argument for a late (Neoproterozoic) onset of plate tectonics is the lacking evidence for ophiolites, low *T/P* rocks, and UHP rocks from the geological record prior to that time (Stern, 2005). Important to note is that low *T/P* and UHP rocks define the modern-style of plate tectonics that includes cold and deep subduction, and not plate tectonics in general which may has operated with global-scale subduction under warmer conditions and shallower depths (Brown, 2006; Sizova et al., 2010, 2014; Hawkesworth et al., 2016; Brown and Johnson, 2018; Holder et al., 2019) in response to higher potential mantle temperatures (Davies, 2009; Korenaga, 2013; Condie et al., 2016; Ganne and Feng, 2017). Thus, the Neoproterozoic can only be considered as may marking the onset of modern-style plate tectonics. However, pre-Neoproterozoic ophiolites exist (Scott et al., 1992; Peltonen et al., 1996; Dann, 1997) and many works report Paleoproterozoic low *T/P* rocks indicative for modern-style plate tectonics (Möller et al., 1995; Collins et al., 2004; Mints et al., 2010; Ganne et al., 2012; Dokukina et al., 2014; Glassley et al., 2014; Perchuk and Morgunova, 2014; Weller and St-Onge, 2017; François et al., 2018; Müller et al., 2018a, 2018b; Xu et al., 2018; de Oliveira Chaves and Porcher, 2020). In addition, a lower proportion of low *T/P* rocks in the pre-Neoproterozoic may be related to the fragmentary geological record through time (e.g. Goodwin, 1996), including biased preservation due to erosion, retrograde metamorphism, and supercontinent cycles (e.g. Wei and Clarke, 2011; Cawood and Hawkesworth, 2014; Weller and St-Onge, 2017; Keller and Schoene, 2018; Chowdhury et al., 2021).

In conclusion, indications for modern-style plate tectonics in the Paleoproterozoic are convincing, but whether these are local or global phenomena and whether deep subduction to UHP conditions was involved are unresolved issues, especially when considering the fragmentary

crystalline rock record (e.g. Goodwin, 1996), the supposed higher metamorphic gradients (Holder et al., 2019), and the oldest evidence for UHP metamorphism in the form of coesite at ~620 Ma (Jahn et al., 2001). To tackle these issues, large regions have to be screened on the presence of low *T/P* and UHP rocks and also material sourced from eroded orogens should be considered to utilize the entire geological record. As targeted field mapping and thin-section analysis to find UHP relicts suffers in screening large rock volumes and is limited to the preserved crystalline rock record, benefits of the technique of analyzing inclusions in detrital minerals (e.g. garnet), as reviewed here, are becoming increasingly important. Thus, this method represents a complimentary and preferable approach to trace UHP metamorphism, and consequently modern-style plate tectonics, through the Precambrian geological record.

5.3. Elastic thermobarometry

By considering the elastic interactions between mineral host–inclusion pairs, elastic thermobarometry aims in determining the *P*–*T* conditions of inclusion entrapment. Because this method is independent from chemical equilibrium of a mineral assemblage (Angel et al., 2015; Mazzucchelli et al., 2018), it is particularly attractive for estimating *P*–*T* conditions of host-mineral crystallization in the UHP field, where phase transformations are rare and only roughly reflect minimal conditions, i.e. >2.9 GPa for coesite, >4 GPa for diamond, and >7 GPa for stishovite at T = 800 °C (e.g. Bundy, 1980; Bose and Ganguly, 1995; Yong et al., 2012). In addition, elastic thermobarometry can be applied to detrital inclusion-bearing mineral grains that otherwise mainly lost their paragenetic context (Baldwin et al., 2021). Such elastic approaches require (i) knowledge of the essential host–inclusion parameters, which includes the equation of state parameters, the elastic tensor, and the phonon-mode Grüneisen tensor (Angel et al., 2014, 2019); and (ii) determination of inclusion strains resulting from different thermoelastic properties of host–inclusion pairs, calculation of the mean stress (i.e. inclusion pressure), and calculation of the isomeke, that is a curve in *P*–*T* space along which both the host and inclusion have the same fractional volume change and therefore are in mechanical equilibrium (Angel et al., 2015, 2017, 2019; Murri et al., 2018; Mazzucchelli et al., 2021). These

elastic models are successfully developed for elastically anisotropic mineral inclusions, such as quartz and zircon, entrapped in a quasi-elastically isotropic host minerals, such as garnet and diamond, and applied in several studies and in combination with other thermobarometric methods (e.g. Gonzalez et al., 2019, 2020; Zhong et al., 2019; Alvaro et al., 2020; Spear and Wolfe, 2020).

The field of elastic thermobarometry is developing rapidly, and a recently introduced theoretical model for anisotropic mineral inclusions in anisotropic host minerals by Gonzalez et al. (2021) gives cause for optimism to study more complex host–inclusion systems in future. However, the subject of coesite-in-garnet has not been touched so far. First of all, the elastic properties of coesite are anomalous and poorly constrained (Angel et al., 2001, 2003; Chen et al., 2015). Secondly, the partially strongly anharmonic behavior and lower symmetry of coesite (monoclinic) compared to quartz (trigonal, hexagonal) and zircon (tetragonal) require complex and resource-intense density-functional theory simulations to determine the phonon-mode Grüneisen tensor components (e.g. Zicovich-Wilson et al., 2004; Prencipe et al., 2012). In addition, the lower symmetry of coesite introduces further complexity to determine the unit cell parameters via single-crystal x-ray diffraction. Thirdly, motivations have probably been hampered because it has been shown that optically monomineralic coesite inclusions often turned out to be bimineralic (coesite + quartz) when investigated by detailed Raman imaging, making the host-inclusion system a complex three-shelled model (e.g. Korsakov et al., 2007; Zhukov and Korsakov, 2015). However, transmission electron microscopy proved the occurrence of monomineralic coesite in kyanite (Taguchi et al., 2019) and garnet (Taguchi et al., 2021) of crystalline rocks from the Sulu Orogen and the Western Alps, making a two-component host–inclusion model sufficient.

The common occurrence of monomineralic coesite in the detrital garnet fraction (Schönig et al., 2018a, 2019, 2020, 2021b; Baldwin et al., 2021) highlight the efficiency of the detrital approach to find a statistically significant number of monomineralic coesite inclusions. We hope this encourages experts to tackle the issue of elastic coesite-in-garnet thermobarometry, potentially providing new insights into the *P*–*T* evolution of UHP rocks, particularly when combined with titanium-in-coesite thermometry (Osborne et al., 2019).

6. Summary

UHP metamorphism is directly linked to deep subduction processes characteristic for modern-style plate tectonics. Studying rocks that experienced these extreme conditions through time has so far been limited to the investigation of crystalline rocks. The novel approach of considering the sedimentary record as an archive for UHP metamorphism was recently introduced by Schönig et al. (2018a, 2019), and further applied by Schönig et al. (2020, 2021b) and Baldwin et al. (2021). These studies report the first findings of the unequivocal mineral indicators for UHP metamorphism, i.e. coesite and diamond, as inclusions in detrital single garnet grains sourced from crustal rocks. Mineral chemistry and co-existing inclusions of the garnets are useful to characterize and discriminate different source lithologies, for instance felsic *vs.* mafic. The method of analyzing the detritus has several benefits compared to sampling crystalline rocks, mainly with regard to reducing the subjectivity of point sampling and the number of samples needed to cover large rock volumes, and the possibility to detect UHP terranes that have been exposed to the Earth's surface in the geological past. The possibilities of a mantle origin and/or recycling have to be carefully considered before linking the detrital signal to deep subduction processes of a specific metamorphic event. Whereas garnet chemistry is appropriate to distinguish between crustal and mantle origin, the effect of recycling is more difficult to handle and depends on the specific case study. In general, the detritus can provide an overview of the characteristics and distribution of UHP rocks and/or their erosional products. UHP detritus may be linked to deep subduction processes of a specific orogenic event and may be used to plan further investigation of the crystalline rock record, provided that they have not yet been eroded.

Future enhancements of the method include a reduction of the analytical time needed and increasing the information value obtained from the detrital UHP grains. This will be achieved by focusing on garnets of a specific grain-size range and composition, and by considering ultrastable minerals as hosts for UHP inclusions. Zircon, rutile, and tourmaline offer great potential for source rock discrimination, geochronology, and thermochronology. In particular, *in situ* geochronologic methods are important to assign detrital grains containing UHP inclusions to a specific metamorphic event. In addition, hyperspectral Raman imaging represents an option to reduce the user-assisted analytical time.

Overall, the findings and potential enhancements regarding the method of tracing UHP metamorphism in the sedimentary record provide an effective and complimentary approach for capturing the distribution and characteristics of UHP rocks exposed on the Earth's surface at the time of sediment generation and deposition. This opens new opportunities to search for UHP events in Earth's history and study the exhumation of UHP terranes. Furthermore, the abundance of monomineralic coesite inclusions in detrital mineral grains enables to systematically study the coesite-to-quartz transformation and coesite preservation during exhumation. We may speculate that monomineralic coesite inclusions could allow to perform elastic thermobarometry in the future.

Acknowledgements

This work was supported by the German Research Foundation [DFG grant EY 23/27-1]. We thank Suzanne L. Baldwin, Joseph P. Gonzalez, Hugh Davies, Raimon Tolosana-Delgado, Arne P. Willner, and Bernhard Schulz for collaboration and discussions during projects intimately related to this contribution. Discussions with Joseph P. Gonzalez regarding host-inclusion systems are gratefully acknowledged and helped improving the manuscript. We thank Michael Brown and an anonymous reviewer for detailed and valuable comments and Yan Wang for the editorial work.

Author contributions

JS Conceptualization, Formal analysis, Investigation, Writing – Original draft, Visualization; **HvE** Conceptualization, Writing – Review and editing, Supervision, Project administration, Funding acquisition; **GM** Conceptualization, Writing – Review and editing, Supervision, Funding acquisition; **NKL** Software, Writing – Review and editing.

References

Agangi, A., Reddy, S.M., Plavsa, D., Fougerouse, D., Clark, C., Roberts, M., Johnson, T.E. 2019. Antimony in rutile as a pathfinder for orogenic gold deposits. Ore Geol. Rev. 106, 1–11. https://doi.org/10.1016/j.oregeorev.2019.01.018

Alvaro, M., Mazzucchelli, M.L., Angel, R.J., Murri, M., Campomenosi, N., Scambelluri, M., Nestola, F., Korsakov, A., Tomilenko, A.A., Marone, F., Morana, M., 2020. Fossil subduction recorded by quartz from the coesite stability field. Geology 48, 24–28. https://doi.org/10.1130/G46617.1

Andò, S., Morton, A., Garzanti, E., 2014. Metamorphic grade of source rocks revealed by chemical fingerprints of detrital amphibole and garnet. In: Scott, R.A., Smyth, H.R., Morton, A.C., Richardson, N. (Eds.), Sediment Provenance Studies in Hydrocarbon Exploration and Production. Geol. Soc. London Spec. Publ. 386, 351–371. https://doi.org/10.1144/SP386.5

Angel, R.J., Mosenfelder, J.L., Shaw, C.S.J., 2001. Anomalous compression and equation of state of coesite. Phys. Earth Planet. Inter. 124, 71–79. https://doi.org/10.1016/S0031-9201(01)00184-4

Angel, R.J., Shaw, C.S.J., Gibbs, G.V., 2003. Compression mechanisms of coesite. Phys. Chem. Miner. 30, 167–176. https://doi.org/10.1007/s00269-003-0303-9

Angel, R.J., Mazzucchelli, M.L., Alvaro, M., Nimis, P., Nestola, F., 2014. Geobarometry from host-inclusion systems: the role of elastic relaxation. Am. Mineral. 99, 2146–2149. https://doi.org/10.2138/am-2014-5047

Angel, R.J., Nimis, P., Mazzucchelli, M.L., Alvaro, M., Nestola, F., 2015. How large are departures from lithostatic pressure? Constraints from host–inclusion elasticity. J. Metamorph. Geol. 33, 801–813. https://doi.org/10.1111/jmg.12138

Angel, R.J., Mazzucchelli, M.L., Alvaro, M., Nestola, F., 2017. EosFit-Pinc: A simple GUI for host-inclusion elastic thermobarometry. Am. Mineral. 102, 1957–1960. https://doi.org/10.2138/am-2017-6190.

Angel, R.J., Murri, M., Mihailova, B., Alvaro, M., 2019. Stress, strain and Raman shifts. Z. Kristallogr. Cryst. Mater. 234, 129–140. https://doi.org/10.1515/zkri-2018-2112

Aubrecht, R., Meres, S., Sýkora, M., Mikus, T., 2009. Provenance of the detrital garnets and spinels from the Albian sediments of the Czorsztyn Unit (Pieniny Klippen Belt, Western Carpathians, Slovakia). Geol. Carpath. 60, 463–483. https://doi.org/10.2478/v10096-009-0034-z

Avigad, D., Nie, S., Yin, A., Rowley, D.B., Jin, Y., 1995. Exhumation of the Dabie Shan ultra–high-pressure rocks and accumulation of the Songpan-Ganzi flysch sequence, central China: Comment and Reply. Geology 23, 764–766.

Baldwin, S.L., Monteleone, B.D., Webb, L.E., Fitzgerald, P.G., Grove, M., Hill, E.J., 2004. Pliocene eclogite exhumation at plate tectonic rates in eastern Papua New Guinea. Nature 431, 263–267. https://doi.org/10.1038/nature02846

Baldwin, S.L., Webb, L.E., Monteleone, B.D., 2008. Late Miocene coesite-eclogite exhumed in the Woodlark Rift. Geology 36, 735–738. https://doi.org/10.1130/G25144A.1

Baldwin, S.L., Fitzgerald, P.G., Webb, L.E., 2012. Tectonics of the New Guinea region. Annu. Rev. Earth Planet. Sci. 40, 495–520. https://doi.org/10.1146/annurev-earth-040809-152540

Baldwin, S.L., Schönig, J., Gonzalez, J.P., Davies, H., von Eynatten, H., 2021. Garnet sand reveals rock recycling processes in the youngest exhumed high- and ultrahigh-pressure terrane on Earth. Proc. Natl. Acad. Sci. 118, e2017231118. https://doi.org/10.1073/pnas.2017231118

Balica, C., Ducea, M.N., Gehrels, G.E., Kirk, J., Roban, R.D., Luffi, P., Chapman, J.B., Triantafyllou, A., Guo, J., Stoica, A.M., Ruiz, J., 2020. A zircon petrochronologic view on granitoids and continental evolution. Earth Planet. Sci. Lett. 531, 116005. https://doi.org/10.1016/j.epsl.2019.116005

Bebout, G.E., Nakamura, E., 2003. Record in metamorphic tourmalines of subduction-zone devolatilization and boron cycling. Geology 31, 407–410. https://doi.org/10.1130/0091-7613(2003)031<0407:RIMTOS>2.0.CO;2

Belousova, E.A., Griffin, W.L., Pearson, N.J., 1998. Trace element composition and cathodoluminescence properties of southern African kimberlitic zircons. Mineral. Mag. 62, 355–366. https://doi.org/10.1180/002646198547747

Belousova, E.A., Kostitsyn, Y.A., Griffin, W.L., Begg, G.C., O'Reilly, S.Y., Pearson, N.J., 2010. The growth of the continental crust: constraints from zircon Hf-isotope data. Lithos 119, 457–466 https://doi.org/10.1016/j.lithos.2010.07.024

Belousova, E.A., Griffin, W.L., O'Reilly, S.Y., Fisher, N.I., 2002. Igneous zircon: trace element composition as an indicator of source rock type. Contrib. Mineral. Petrol. 143, 602–622. https://doi.org/10.1007/s00410-002-0364-7

Bercovici, D., Ricard, Y., 2014. Plate tectonics, damage and inheritance. Nature 508, 513–516. https://doi.org/10.1038/nature13072

Bernet, M., van der Beek, P., Pik, R., Huyghe, P., Mugnier, J.L., Labrinz, E., Szulc, A., 2006. Miocene to Recent exhumation of the central Himalaya determined from combined detrital zircon fission track and U/Pb analysis of Siwalik sediments, western Nepal: Basin Res. 18, 393–412. https://doi.org/10.1111/j.1365-2117.2006.00303.x

Blackburn, T., Bowring, S., Schoene, B., Mahan, K., Dudas, F., 2011. U–Pb thermochronology: creating a temporal record of lithosphere thermal evolution. Contrib. Mineral. Petrol. 162, 479–500. https://doi.org/10.1007/s00410-011-0607-6

Bose, K., Ganguly, J., 1995. Quartz-coesite transition revisited: Reversed experimental determination at 500–1200 °C and retrieved thermochemical properties. Am. Mineral. 80, 231–238. https://doi.org/10.2138/am-1995-3-404

Brown, M., 2006. Duality of thermal regimes is the distinctive characteristic of plate tectonics since the Neoarchean. Geology 34, 961–964. https://doi.org/10.1130/G22853A.1

Brown, M., 2014. The contribution of metamorphic petrology to understanding lithosphere evolution and geodynamics. Geosci. Front. 5, 553–569. https://doi.org/10.1016/j.gsf.2014.02.005

Brown, M., Johnson, T., 2018. Secular change in metamorphism and the onset of global plate tectonics. Am. Mineral. 103, 181–196. https://doi.org/10.2138/am-2018-6166

Brown, M., Johnson, T., Gardiner, N.J., 2020. Plate tectonics and the Archean Earth. Annu. Rev. Earth Planet. Sci. 48, 291–320. https://doi.org/10.1146/annurev-earth-081619-052705

Bruguier, O., Bosch, D., Caby, R., Vitale-Brovarone, A., Fernandez, L., Hammor, D., Laouar, R., Ouabadi, A., Abdallah, N., Mechati, M., 2017. Age of UHP metamorphism in the Western Mediterranean: insight from rutile and minute zircon inclusions in a diamond-bearing garnet megacryst (Edough Massif, NE Algeria). Earth Planet. Sci. Lett. 474, 215–225. https://doi.org/10.1016/j.epsl.2017.06.043

Bundy, F.P., 1980. The P, T phase and reaction diagram for elemental carbon, 1979. J. Geophys. Res. Solid Earth 85, 6930–6936. https://doi.org/10.1029/JB085iB12p06930

Burov, E., Cloetingh, S., 2010. Plume-like upper mantle instabilities drive subduction initiation. Geophys. Res. Lett. 37, L03309. https://doi.org/10.1029/2009GL041535

Campbell, I.H., Reiners, P.W., Allen, C.M., Nicolescu, S., Upadhyay, R., 2005. He–Pb double dating of detrital zircons from the Ganges and Indus Rivers: implication for quantifying sediment recycling and provenance studies. Earth Planet. Sci. Lett. 237, 402–432. https://doi.org/10.1016/j.epsl.2005.06.043

Carson, C.J., Ague, J.J., Coath, C.D., 2002. U–Pb geochronology from Tonagh Island, East Antarctica: implications for the timing of ultra-high temperature metamorphism of the Napier Complex. Precambrian Res. 116, 237–263. https://doi.org/10.1016/S0301-9268(02)00023-2

Carswell, D.A., Compagnoni, R., 2003. Introduction with review of the definition, distribution and geotectonic significance of ultrahigh pressure metamorphism. In: Carswell, D.A., Compagnoni, R. (Eds.), Ultrahigh Pressure Metamorphism, 5. EMU Notes in Mineralogy, pp. 3–9.

Carter, A., Moss, S.J., 1999. Combined detrital-zircon fission-track and U-Pb dating: A new approach to understanding hinterland evolution. Geology 27, 235–238. https://doi.org/10.1130/0091-7613(1999)027<0235:CDZFTA>2.3.CO;2

Cawood, P.A., Hawkesworth, C.J., 2014. Earth's middle age. Geology 42, 503–506. https://doi.org/10.1130/G35402.1

Cawood, P.A., Kroner, A., Pisarevsky, S., 2006. Precambrian plate tectonics: criteria and evidence. GSA Today 16, 4–11. https://doi.org/10.1130/GSAT01607.1

Chao, E.C., Shoemaker, E.M., Madsen, B.M., 1960. First natural occurrence of coesite. Science 132, 220–222. https://doi.org/10.1126/science.132.3421.220

Chen, Z., Zhou, J., Li, R., Wan, Y., 2005. Mineral inclusions and internal structure of detrital zircons from lower Jurassic sedimentary rocks of Fanghushan Formation in Hefei Basin. Acta Mineral. Sinica 25, 89–96.

Chen, T., Gwanmesia, G.D., Wang, X., Zou, Y., Liebermann, R.C., Michaut, C., Li, B., 2015. Anomalous elastic properties of coesite at high pressure and implications for the upper mantle X-discontinuity. Earth Planet. Sci. Lett. 412, 42–51. https://doi.org/10.1016/j.epsl.2014.12.025

Chopin, C., 1984. Coesite and pure pyrope in high-grade blueschists of the Western Alps: a first record and some consequences. Contrib. Mineral. Petrol. 86, 107–118. https://doi.org/10.1007/BF00381838

Chopin, C., 2003. Ultrahigh-pressure metamorphism: tracing continental crust into the mantle. Earth Planet. Sci. Lett. 212, 1–14. https://doi.org/10.1016/S0012-821X(03)00261-9

Chowdhury, P., Chakraborty, S., Gerya, T.V., 2021. Time can tell: Secular change in metamorphic timescales and the tectonic implications. Gondwana Res. 93, 291–310. https://doi.org/10.1016/j.gr.2021.02.003

Clark, J.R., Williams-Jones, A.E., 2004. Rutile as a potential indicator mineral for metamorphosed metallic ore deposits. Rapport Final de DIVEX, Sous-project SC2, Montréal, Canada, pp. 17.

Collins, A.S., Reddy, S.M., Buchan, C., Mruma, A., 2004. Temporal constraints on Palaeoproterozoic eclogite formation and exhumation (Usagaran Orogen, Tanzania). Earth Planet. Sci. Lett. 224, 175–192. https://doi.org/10.1016/j.epsl.2004.04.027

Condie, K.C., Aster, R.C., van Hunen, J., 2016. A great thermal divergence in the mantle beginning 2.5 Ga: Geochemical constraints from greenstone basalts and komatiites. Geosci. Front. 7, 543–553. https://doi.org/10.1016/j.gsf.2016.01.006

Conrad, C.P., Lithgow-Bertelloni, C., 2002. How mantle slabs drive plate tectonics. Science 298, 207–209. https://doi.org/10.1126/science.1074161

Cookenboo, H.O., Bustin, R.M., Wilks, K.R., 1997. Detrital chromian spinel compositions used to reconstruct the tectonic setting of provenance; implications for orogeny in the Canadian Cordillera. J. Sediment. Res. 67, 116–123.

Corfu, F., Hanchar, J.M., Hoskin, P.W., Kinny, P., 2003. Atlas of zircon textures. Rev. Mineral. Geochem. 53, 469–500.

Cuthbert, S.J., 1991. Evolution of the Devonian Hornelen Basin, west Norway: new constraints from petrological studies of metamorphic clasts. In: Morton, A.C., Todd, S.P., Haughton, P.D.W. (Eds.), Developments in Sedimentary Provenance Studies. Geol. Soc. London Spec. Publ. 57, pp. 343–360. https://doi.org/10.1144/GSL.SP.1991.057.01.25

Dahl, P.S., 1997. A crystal-chemical basis for Pb retention and fission-track annealing systematics in U-bearing minerals, with implications for geochronology. Earth Planet. Sci. Lett. 150, 277–290. https://doi.org/10.1016/S0012-821X(97)00108-8

Dann, J.C., 1997. Pseudostratigraphy and origin of the Early Proterozoic Payson ophiolite, central Arizona. GSA Bulletin 109, 347–365. https://doi.org/10.1130/0016-7606(1997)109<0347:PAOOTE>2.3.CO;2

Davaille, A., Smrekar, S.E., Tomlinson, S., 2017. Experimental and observational evidence for plume-induced subduction on Venus. Nat. Geosci. 10, 349–355. https://doi.org/10.1038/ngeo2928

Davies, G.F., 2009. Effect of plate bending on the Urey ratio and the thermal evolution of the mantle. Earth Planet. Sci. Lett. 287, 513–518. https://doi.org/10.1016/j.epsl.2009.08.038

de Oliveira Chaves, A., Porcher, C.C., 2020. Petrology, geochemistry and Sm-Nd systematics of the Paleoproterozoic Itaguara retroeclogite from São Francisco/Congo Craton: one of the oldest records of the modern-style plate tectonics. Gondwana Res. 87, 224–237. https://doi.org/10.1016/j.gr.2020.06.014

Dewey, J.F., Kiseeva, E.S., Pearce, J.A., Robb, L.J., 2021. Precambrian tectonic evolution of Earth: an outline. S. Afr. J. Geol. 124, 141–162. https://doi.org/10.25131/sajg.124.0019

Dhuime, B., Hawkesworth, C.J., Cawood, P.A., Storey, C.D., 2012. A change in the geodynamics of continental growth 3 billion years ago. Science 335, 1334–1336. https://doi.org/10.1126/science.1216066

Dhuime, B., Wuestefeld, A., Hawkesworth, C.J., 2015. Emergence of modern continental crust about 3 billion years ago. Nat. Geosci. 8, 552–555. https://doi.org/10.1038/ngeo2466

Dhuime, B., Hawkesworth, C.J., Delavault, H., Cawood, P.A., 2017. Continental growth seen through the sedimentary record. Sediment. Geol. 357, 16–32. https://doi.org/10.1016/j.sedgeo.2017.06.001

Dick, H.J., Bullen, T., 1984. Chromian spinel as a petrogenetic indicator in abyssal and alpine-type peridotites and spatially associated lavas. Contrib. Mineral. Petrol. 86, 54–76. https://doi.org/10.1007/BF00373711

Dobrzhinetskaya, L., Wirth, R., Green, H., 2014. Diamonds in Earth's oldest zircons from Jack Hills conglomerate, Australia, are contamination. Earth Planet Sci Lett 387, 212–218. https://doi.org/10.1016/j.epsl.2013.11.023

Dokukina, K.A., Kaulina, T.V., Konilov, A.N., Mints, M.V., Van, K.V., Natapov, L., Belousova, E., Simakin, S.G., Lepekhina, E.N., 2014. Archaean to Palaeoproterozoic high-grade evolution of the Belomorian eclogite province in the Gridino area, Fennoscandian Shield: Geochronological evidence. Gondwana Res. 25, 585–613. https://doi.org/10.1016/j.gr.2013.02.014

Dunkl, I., Frisch, W., Kuhlemann, J., Brügel, A., 2009. Pebble population dating as an additional tool for provenance studies — examples from the Eastern Alps. In: Lisker, F., Ventura, B., Glasmacher, U.A. (Eds.), Thermochronological Methods: From Palaeotemperature Constraints to Landscape Evolution Models. Geol. Soc. London Spec. Publ. 324, pp. 125–140. https://doi.org/10.1144/SP324.10

Enkelmann, E., Weislogel, A., Ratschbacher, L., Eide, E., Renno, A., Wooden, J., 2007. How was the Triassic Songpan-Ganzi basin filled? A provenance study. Tectonics 26, TC4007. https://doi.org/10.1029/2006TC002078

Enkelmann, E., Garver, J.I., Pavlis, T.L., 2008. Rapid exhumation of ice-covered rocks of the Chugach–St. Elias orogen, Southeast Alaska. Geology 36, 915–918. https://doi.org/10.1130/G2252A.1

Ernst, W.G., 2006. Preservation/exhumation of ultrahigh-pressure subduction complexes. Lithos 92, 321–335. https://doi.org/10.1016/j.lithos.2006.03.049

Ernst, W.G., 2017. Earth's thermal evolution, mantle convection, and Hadean onset of plate tectonics. J. Asian Earth Sci. 145, 334–348. https://doi.org/10.1016/j.jseaes.2017.05.037

Ertl, A., Marschall, H.R., Giester, G., Henry, D.J., Schertl, H.P., Ntaflos, T., Luvizotto, G.L., Nasdala, L., Tillmanns, E., 2010. Metamorphic ultrahigh-pressure tourmaline: Structure, chemistry, and correlations to P-T conditions. Am. Mineral. 95, 1–10. https://doi.org/10.2138/am.2010.3283

Evans, N.J., McInnes, B.I.A., McDonald, B., Danišík, M., Jourdan, F., Mayers, C., Thern, E., Corbett, D., 2013. Emplacement age and thermal footprint of the diamondiferous Ellendale E9 lamproite pipe, Western Australia. Miner. Depos. 48, 413–421. https://doi.org/10.1007/s00126-012-0430-7

Ewing, T.A., Hermann, J., Rubatto, D., 2013. The robustness of the Zr-in-rutile and Ti-in-zircon thermometers during high-temperature metamorphism (Ivrea-Verbano Zone, northern Italy). Contrib. Mineral. Petrol. 165, 757–779. 10.1007/s00410-012-0834-5

Faryad, S.W., Cuthbert, S.J., 2020. High-temperature overprint in (U)HPM rocks exhumed from subduction zones; A product of isothermal decompression or a consequence of slab break-off (slab rollback)? Earth-Sci. Rev. 202, 103108. https://doi.org/10.1016/j.earscirev.2020.103108

Faryad, S.W., Baldwin, S.L., Jedlicka, R., Ježek, J., 2019. Two-stage garnet growth in coesite eclogite from the southeastern Papua New Guinea (U)HP terrane and its geodynamic significance. Contrib. Mineral. Petrol. 174, 1–16. https://doi.org/10.1007/s00410-019-1612-4

Ferrière, L., Osinski, G.R., 2012. Shock metamorphism. In: Osinski, G.R., Pierazzo, E. (Eds.), Impact Cratering: Processes and Products. John Wiley & Sons, 106–124.

Ferry, J.M., Watson, E.B., 2007. New thermodynamic models and revised calibrations for the Ti-in-zircon and Zr-in-rutile thermometers. Contrib. Mineral. Petrol. 154, 429–437. https://doi.org/10.1007/s00410-007-0201-0

Field, M., Stiefenhofer, J., Robey, J., Kurszlaukis, S., 2008. Kimberlite-hosted diamond deposits of southern Africa: a review. Ore Geol. Rev. 34, 33–75.

Force, E.R., 1980. The provenance of rutile. J. Sediment. Res. 50, 485–488. https://doi.org/10.1306/212F7A31-2B24-11D7-8648000102C1865D

Forsyth, D., Uyeda, S., 1975. On the relative importance of the driving forces of plate motion. Geophys. J. Int. 43, 163–200. https://doi.org/10.1111/j.1365-246X.1975.tb00631.x

Frei, D., Gerdes, A., 2009. Precise and accurate in situ U–Pb dating of zircon with high sample throughput by automated LA-SF-ICP-MS. Chem. Geol. 261, 261–270. https://doi.org/10.1016/j.chemgeo.2008.07.025

Fornelli, A., Langone, A., Micheletti, F., Pascazio, A., Piccarreta, G., 2014. The role of trace element partitioning between garnet, zircon and orthopyroxene on the interpretation of zircon U–Pb ages: an example from high-grade basement in Calabria (Southern Italy). Int. J. Earth Sci. 103, 487–507. https://doi.org/10.1007/s00531-013-0971-8

François, C., Debaille, V., Paquette, J.L., Baudet, D., Javaux, E.J., 2018. The earliest evidence for modern-style plate tectonics recorded by HP–LT metamorphism in the Paleoproterozoic of the Democratic Republic of the Congo. Sci. Rep. 8, 15452. https://doi.org/10.1038/s41598-018-33823-y

French, B.M., Koeberl, C., 2010. The convincing identification of terrestrial meteorite impact structures: What works, what doesn't, and why. Earth-Sci. Rev. 98, 123–170. https://doi.org/10.1016/j.earscirev.2009.10.009

Ganne, J., Feng, X., 2017. Primary magmas and mantle temperatures through time. Geochemistry, Geophys., Geosystems 18, 872–888. https://doi.org/10.1002/2016GC006787

Ganne, J., De Andrade, V., Weinberg, R.F., Vidal, O., Dubacq, B., Kagambega, N., Naba, S., Baratoux, L., Jessell, M., Allibon, J., 2012. Modern-style plate subduction preserved in the Palaeoproterozoic West African craton. Nat. Geosci. 5, 60–65. https://doi.org/10.1038/ngeo1321

Gauthiez-Putallaz, L., Rubatto, D., Hermann, J., 2016. Dating prograde fluid pulses during subduction by in situ U–Pb and oxygen isotope analysis. Contrib. Mineral. Petrol. 171, 15. 10.1007/s00410-015-1226-4

Gebauer, D., Schertl, H.P., Brix, M., Schreyer, W., 1997. 35 Ma old ultrahigh-pressure metamorphism and evidence for very rapid exhumation in the Dora Maira Massif, Western Alps. Lithos 41, 5–24. https://doi.org/10.1016/S0024-4937(97)82002-6

Gerya, T.V., Stern, R.J., Baes, M., Sobolev, S.V., Whattam, S.A., 2015. Plate tectonics on the Earth triggered by plume-induced subduction initiation. Nature 527, 221–225. https://doi.org/10.1038/nature15752

Glassley, W.E., Korstgård, J.A., Sørensen, K., Platou, S.W., 2014. A new UHP metamorphic complex in the ~1.8 Ga Nagssugtoqidian Orogen of West Greenland. Am. Mineral. 99, 1315–1334. https://doi.org/10.2138/am.2014.4726

Gonzalez, J.P., Thomas, J.B., Baldwin, S.L., Alvaro, M., 2019. Quartz-in-garnet and Ti-in-quartz thermobarometry: Methodology and first application to a quartzofeldspathic gneiss from eastern Papua New Guinea. J. Metamorph. Geol. 37, 1193–1208. https://doi.org/10.1111/jmg.12508

Gonzalez, J.P., Baldwin, S.L., Thomas, J.B., Nachlas, W.O. and Fitzgerald, P.G., 2020. Evidence for ultrahigh-pressure metamorphism discovered in the Appalachian orogen. Geology 48, 947–951. https://doi.org/10.1130/G47507.1

Gonzalez, J.P., Mazzucchelli, M.L., Angel, R.J., Alvaro, M., 2021. Elastic Geobarometry for Anisotropic Inclusions in Anisotropic Host Minerals: Quartz-in-Zircon. J. Geophys. Res. Solid Earth 126, 2021JB022080. https://doi.org/10.1029/2021JB022080

Goodwin, A.M., 1996. Principles of Precambrian geology. Academic Press London, pp. 327.

Gose, J., Schmädicke, E., 2018. Water incorporation in garnet: Coesite versus quartz eclogite from Erzgebirge and Fichtelgebirge. J. Petrol. 59, 207–232. https://doi.org/10.1093/petrology/egy022

Greber, N.D., Dauphas, N., Bekker, A., Ptáček, M.P., Bindeman, I.N., Hofmann, A., 2017. Titanium isotopic evidence for felsic crust and plate tectonics 3.5 billion years ago. Science 357, 1271–1274. https://doi.org/10.1126/science.aan8086

Grimes, C.B., Wooden, J.L., Cheadle, M.J., John, B.E., 2015. "Fingerprinting" tectono-magmatic provenance using trace elements in igneous zircon. Contrib. Mineral. Petrol. 170, 1–26. https://doi.org/10.1007/s00410-015-1199-3

Grimmer, J.C., Ratschbacher, L., McWilliams, M., Franz, L., Gaitzsch, I., Tichomirowa, M., Hacker, B.R., Zhang, Y., 2003. When did the ultrahigh-pressure rocks reach the surface? A $^{207}Pb/^{206}Pb$ zircon, $^{40}Ar/^{39}Ar$ white mica, Si-in-white mica, single-grain provenance study of Dabie Shan synorogenic foreland sediments. Chem. Geol. 197, 87–110. https://doi.org/10.1016/S0009-2541(02)00321-2

Grütter, H.S., Gurney, J.J., Menzies, A.H., Winter, F., 2004. An updated classification scheme for mantle-derived garnets, for use by diamond explorers. Lithos 77, 841–857. https://doi.org/10.1016/j.lithos.2004.04.012

Guo, R., Hu, X., Garzanti, E., Lai, W., 2021. Boron isotope composition of detrital tourmaline: A new tool in provenance analysis. Lithos 400, 106360. https://doi.org/10.1016/j.lithos.2021.106360

Gurnis, M., Hall, C., Lavier, L., 2004. Evolving force balance during incipient subduction. Geochemistry, Geophys., Geosystems 5, Q07001. https://doi.org/10.1029/2003GC000681

Gurney, J.J., Zweistra, P., 1995. The interpretation of the major element compositions of mantle minerals in diamond exploration. J. Geochem. Explor. 53, 293–309. https://doi.org/10.1016/0375-6742(94)00021-3

Hacker, B.R., Ratschbacher, L., Webb, L., Ireland, T., Walker, D., Shuwen, D., 1998. U/Pb zircon ages constrain the architecture of the ultrahigh-pressure Qinling–Dabie Orogen, China. Earth Planet. Sci. Lett. 161, 215–230. https://doi.org/10.1016/S0012-821X(98)00152-6

Hamilton, W.B., 2011. Plate tectonics began in Neoproterozoic time, and plumes from deep mantle have never operated. Lithos 123, 1–20. https://doi.org/10.1016/j.lithos.2010.12.007

Han, S., Li, M., Ren, Q., 2019. Discriminating among tectonic settings of spinel based on multiple machine learning algorithms. Big Earth Data 3, 67–82. https://doi.org/10.1080/20964471.2019.1586074

Hardman, M.F., Pearson, D.G., Stachel, T., Sweeney, R.J., 2018. Statistical approaches to the discrimination of crust- and mantle-derived low-Cr garnet – Major-element-based methods and their application in diamond exploration. J. Geochem. Explor. 186, 24–35. https://doi.org/10.1016/j.gexplo.2017.11.012

Harley, S.L., Kelly, N.M., Möller, A., 2007. Zircon behaviour and the thermal histories of mountain chains. Elements 3, 25–30. https://doi.org/10.2113/gselements.3.1.25

Harrison, T.M., Ryerson, F.J., Le Fort, P., Yin, A., Lovera, O.M., Catlos, E.J., 1997. A late Miocene-Pliocene origin for the central Himalayan inverted metamorphism. Earth Planet. Sci. Lett. 146, E1–E7. https://doi.org/10.1016/S0012-821X(96)00215-4

Hart, E., Storey, C., Bruand, E., Schertl, H.-P., Alexander, B.D., 2016. Mineral inclusions in rutile: A novel recorder of HP-UHP metamorphism. Earth Planet. Sci. Lett. 446, 137–148. https://doi.org/10.1016/j.epsl.2016.04.035

Hart, E., Storey, C., Harley, S.L., Fowler, M., 2018. A window into the lower crust: Trace element systematics and the occurrence of inclusions/intergrowths in granulite-facies rutile. Gondwana Res. 59, 76–86. https://doi.org/10.1016/j.gr.2018.02.021

Hawkesworth, C.J., Cawood, P.A., Dhuime, B., 2016. Tectonics and crustal evolution. GSA Today 26. https://doi.org/10.1130/GSATG272A.1

Henry, D.J., Guidotti, C.V., 1985. Tourmaline as a petrogenetic indicator mineral: an example from the staurolite-grade metapelites of NW Maine. Am. Mineral. 70, 1–15.

Hermann, J., Rubatto, D., Korsakov, A., Shatsky, V.S., 2001. Multiple zircon growth during fast exhumation of diamondiferous, deeply subducted continental crust (Kokchetav Massif, Kazakhstan). Contrib. Mineral. Petrol. 141, 66–82. https://doi.org/10.1007/s004100000218

Hermann, J., Spandler, C., Hack, A., Korsakov, A.V., 2006. Aqueous fluids and hydrous melts in high-pressure and ultra-high pressure rocks: Implications for element transfer in subduction zones. Lithos 92, 399–417. https://doi.org/10.1016/j.lithos.2006.03.055

Hokada, T., Harley, S.L., 2004. Zircon growth in UHT leucosome: constraints from zircon-garnet rare earth elements (REE) relations in Napier Complex, East Antarctica. J. Mineral. Petrol. Sci. 99, 180–190. https://doi.org/10.2465/jmps.99.180

Holder, R.M., Viete, D.R., Brown, M., Johnson, T.E., 2019. Metamorphism and the evolution of plate tectonics. Nature 572, 378–381. https://doi.org/10.1038/s41586-019-1462-2

Holland, T.J., 1980. The reaction albite = jadeite + quartz determined experimentally in the range 600–1200°C. Am. Mineral. 65, 129–134

Hopkins, M., Harrison, T.M., Manning, C.E., 2008. Low heat flow inferred from >4 Gyr zircons suggests Hadean plate boundary interactions. Nature 456, 493–496. https://doi.org/10.1038/nature07465

Hopkins, M.D., Harrison, T.M., Manning, C.E., 2010. Constraints on Hadean geodynamics from mineral inclusions in >4 Ga zircons. Earth Planet. Sci. Lett. 298, 367–376. https://doi.org/10.1016/j.epsl.2010.08.010

Hoskin, P.W., Ireland, T.R., 2000. Rare earth element chemistry of zircon and its use as a provenance indicator. Geology 28, 627–630. https://doi.org/10.1130/0091-7613(2000)28<627:REECOZ>2.0.CO;2

Hubert, J.F., 1962. A zircon-tourmaline-rutile maturity index and the interdependence of the composition of heavy mineral assemblages with the gross composition and texture of sandstones. J. Sediment. Res. 32, 440–450. https://doi.org/10.1306/74D70CE5-2B21-11D7-8648000102C1865D

Ireland, T.R., Williams, I.S., 2003. Considerations in zircon geochronology by SIMS. Rev. Mineral. Geochem. 53, 215–241. https://doi.org/10.2113/0530215

Irvine, T.N., 1967. Chromian spinel as a petrogenetic indicator: Part 2. Petrologic applications. Can. J. Earth Sci. 4, 71–103.

Jahn, B.M., Caby, R., Monie, P., 2001. The oldest UHP eclogites of the World: age of UHP metamorphism, nature of protoliths and tectonic implications. Chem. Geol. 178, 143–158. https://doi.org/10.1016/S0009-2541(01)00264-9

John, T., Schenk, V., 2003. Partial eclogitisation of gabbroic rocks in a late Precambrian subduction zone (Zambia): prograde metamorphism triggered by fluid infiltration. Contrib. Mineral. Petrol. 146, 174–191. https://doi.org/10.1007/s00410-003-0492-8

Keller, B., Schoene, B., 2018. Plate tectonics and continental basaltic geochemistry throughout Earth history. Earth Planet. Sci. Lett. 481, 290–304. https://doi.org/10.1016/j.epsl.2017.10.031

Kellett, D.A., Weller, O.M., Zagorevski, A., Regis, D., 2018. A petrochronological approach for the detrital record: Tracking mm-sized eclogite clasts in the northern Canadian Cordillera. Earth Planet. Sci. Lett. 494, 23–31. https://doi.org/10.1016/j.epsl.2018.04.036

Kelly, N.M., Harley, S.L., 2005. An integrated microtextural and chemical approach to zircon geochronology: refining the Archaean history of the Napier Complex, east Antarctica. Contrib. Mineral. Petrol. 149, 57–84. https://doi.org/10.1007/s00410-004-0635-6

Kohn, M.J., 2020. A refined zirconium-in-rutile thermometer. Am. Mineral. 105, 963–971. https://doi.org/10.2138/am-2020-7091

Kohn, M.J., Corrie, S.L., Markley, C., 2015. The fall and rise of metamorphic zircon. Am. Mineral. 100, 897–908. https://doi.org/10.2138/am-2015-5064

Kohn, B., Chung, L., Gleadow, A., 2019. Fission-track analysis: field collection, sample preparation and data acquisition. In: Malusà, M.G., Fitzgerald, P.G. (Eds.), Fission-Track Thermochronology and its Application to Geology, Springer, Cham, pp. 25–48. https://doi.org/10.1007/978-3-319-89421-8_2

Komiya, T., Maruyama, S., Masuda, T., Nohda, S., Hayashi, M., Okamoto, K., 1999. Plate tectonics at 3.8–3.7 Ga: Field evidence from the Isua accretionary complex, southern West Greenland. J. Geol. 107, 515–554.

Kooijman, E., Mezger, K., Berndt, J., 2010. Constraints on the U–Pb systematics of metamorphic rutile from in situ LA-ICP-MS analysis. Earth Planet. Sci. Lett. 293, 321–330. https://doi.org/10.1016/j.epsl.2010.02.047

Kooijman, E., Smit, M.A., Mezger, K., Berndt, J., 2012. Trace element systematics in granulite facies rutile: implications for Zr geothermometry and provenance studies. J. Metamorph. Geol. 30, 397–412. https://doi.org/10.1111/j.1525-1314.2012.00972.x

Korenaga, J., 2013. Initiation and evolution of plate tectonics on Earth: theories and observations. Annu. Rev. Earth Planet. Sci. 41, 117–151. https://doi.org/10.1146/annurev-earth-050212-124208

Korhonen, F.J., Clark, C., Brown, M., Bhattacharya, S., Taylor, R., 2013. How long-lived is ultrahigh temperature (UHT) metamorphism? Constraints from zircon and monazite geochronology in the Eastern Ghats orogenic belt, India. Precambrian Res. 234, 322–350. https://doi.org/10.1016/j.precamres.2012.12.001

Korsakov, A.V., Hutsebaut, D., Theunissen, K., Vandenabeele, P., Stepanov, A.S., 2007. Raman mapping of coesite inclusions in garnet from the Kokchetav Massif (Northern Kazakhstan): Spectrochim. Acta A, 68, 1046–1052. https://doi.org/10.1016/j.saa.2007.04.005

Kotková, J., O'Brien, P.J., Ziemann, M.A., 2011. Diamond and coesite discovered in Saxony-type granulite: Solution to the Variscan garnet peridotite enigma. Geology 39, 667–670. https://doi.org/10.1130/G31971.1

Krippner, A., Bahlburg, H., 2013. Provenance of Pleistocene Rhine River Middle Terrace sands between the Swiss–German border and Cologne based on U–Pb detrital zircon ages. Int. J. Earth Sci. 102, 917–932. https://doi.org/10.1007/s00531-012-0842-8

Krippner, A., Meinhold, G., Morton, A.C., von Eynatten, H., 2014. Evaluation of garnet discrimination diagrams using geochemical data of garnets derived from various host rocks. Sediment. Geol. 306, 36–52. https://doi.org/10.1016/j.sedgeo.2014.03.004

Krippner, A., Meinhold, G., Morton, A.C., Russell, E., von Eynatten, H., 2015. Grain-size dependence of garnet composition revealed by provenance signatures of modern stream sediments from the

western Hohe Tauern (Austria). Sediment. Geol. 321, 25–38. https://doi.org/10.1016/j.sedgeo.2015.03.002

Krippner, A., Meinhold, G., Morton, A.C., Schönig, J., von Eynatten, H., 2016. Heavy minerals and garnet geochemistry of stream sediments and bedrocks from the Almklovdalen area, Western Gneiss Region, SW Norway: Implications for provenance analysis. Sediment. Geol. 336, 96–105. https://doi.org/10.1016/j.sedgeo.2015.09.009

Kueter, N., Soesilo, J., Fedortchouk, Y., Nestola, F., Belluco, L., Troch, J., Wälle, M., Guillong, M., von Quadt, A., Driesner, T., 2016. Tracing the depositional history of Kalimantan diamonds by zircon provenance and diamond morphology studies. Lithos 265, 159–176.

Li, R., Wan, Y., Cheng, Z., Zhou, J., Li, S., Jin, F., Meng, Q., Li, Z., Jiang, M., 2005. Provenance of Jurassic sediments in the Hefei Basin, east-central China and the contribution of high-pressure and ultrahigh-pressure metamorphic rocks from the Dabie Shan. Earth Planet. Sci. Lett. 231, 279–294. https://doi.org/10.1016/j.epsl.2004.12.021

Linnemann, U., Herbosch, A., Liégeois, J.P., Pin, C., Gärtner, A., Hofmann, M., 2012. The Cambrian to Devonian odyssey of the Brabant Massif within Avalonia: A review with new zircon ages, geochemistry, Sm–Nd isotopes, stratigraphy and palaeogeography. Earth-Sci. Rev. 112, 126–154. https://doi.org/10.1016/j.earscirev.2012.02.007

Liou, J.G., Zhang, A., 1996. Occurrences of intergranular coesite in ultrahigh-P rocks from the Sulu region, eastern China: implications for lack of fluid during exhumation. Am. Mineral. 81, 1217–1221. https://doi.org/10.2138/am-1996-9-1020

Liou, J.G., Ernst, W.G., Zhang, R.Y., Tsujimori, T., Jahn, B.M, 2009. Ultrahigh-pressure minerals and metamorphic terranes – the view from China. J. Asian Earth Sci. 35, 199–231. https://doi.org/10.1016/j.jseaes.2008.10.012

Liu, F., Gerdes, A., Zeng, L., Xue, H., 2008. SHRIMP U–Pb dating, trace elements and the Lu–Hf isotope system of coesite-bearing zircon from amphibolite in the SW Sulu UHP terrane, eastern China. Geochim. Cosmochim. Acta 72, 2973–3000. https://doi.org/10.1016/j.gca.2008.04.007

Liu, P., Massonne, H.J., Zhang, J., Wu, Y., Jin, Z., 2017. Intergranular coesite and coesite inclusions in dolomite from the Dabie Shan: Constraints on the preservation of coesite in UHP rocks. Terra Nova 29, 154–161. https://doi.org/10.1111/ter.12258

Lünsdorf, N.K., Dunkl, I., Schmidt, B.C., Rantitsch, G., von Eynatten, H., 2017. Towards a higher comparability of geothermometric data obtained by Raman spectroscopy of carbonaceous material. Part 2: A revised geothermometer. Geostand. Geoanal. Res. 41, 593–612. https://doi.org/10.1111/ggr.12178

Luvizotto, G.L., Zack, T., 2009. Nb and Zr behavior in rutile during high-grade metamorphism and retrogression: an example from the Ivrea–Verbano Zone. Chem. Geol. 261, 303–317. https://doi.org/10.1016/j.chemgeo.2008.07.023

Luvizotto, G.L., Zack, T., Triebold, S. von Eynatten, H., 2009. Rutile occurrence and trace element behavior in medium-grade metasedimentary rocks: example from the Erzgebirge, Germany. Miner. Petrol. 97, 233–249. 10.1007/s00710-009-0092-z

Maneiro, K.A., Baxter, E.F., Samson, S.D., Marschall, H.R., Hietpas, J., 2019. Detrital garnet geochronology: Application in tributaries of the French Broad River, Southern Appalachian Mountains, USA. Geology 47, 1189–1192. https://doi.org/10.1130/G46840.1

Mange, M.A., Morton, A.C., 2007. Geochemistry of heavy minerals. In: Mange, M.A., Wright, D.T. (Eds.), Dev. Sedimentol. 58, 345–391. https://doi.org/10.1016/S0070-4571(07)58013-1

Marschall, H.R., Jiang, S.Y., 2011. Tourmaline isotopes: no element left behind. Elements 7, 313–319. https://doi.org/10.2113/gselements.7.5.313

Marschall, H.R., Korsakov, A.V., Luvizotto, G.L., Nasdala, L., Ludwig, T., 2009. On the occurrence and boron isotopic composition of tourmaline in (ultra)high-pressure metamorphic rocks. J. Geol. Soc. London 166, 811–823. https://doi.org/10.1144/0016-76492008-042

Martin, A.J., Gehrels, G.E. and DeCelles, P.G., 2007. The tectonic significance of (U,Th)/Pb ages of monazite inclusions in garnet from the Himalaya of central Nepal. Chem. Geol. 244, 1–24. https://doi.org/10.1016/j.chemgeo.2007.05.003

Martínez-Martínez, J.M., Torres-Ruiz, J., Pesquera, A., Gil-Crespo, P.P., 2010. Geological relationships and U–Pb zircon and $^{40}Ar/^{39}Ar$ tourmaline geochronology of gneisses and

tourmalinites from the Nevado–Filabride complex (western Sierra Nevada, Spain): tectonic implications. Lithos 119, 238–250. https://doi.org/10.1016/j.lithos.2010.07.002

Maruyama, S., Santosh, M., Azuma, S., 2018. Initiation of plate tectonics in the Hadean: Eclogitization triggered by the ABEL Bombardment. Geosci. Front. 9, 1033–1048. https://doi.org/10.1016/j.gsf.2016.11.009

Massonne, H.J., 2003. A comparison of the evolution of diamondiferous quartz-rich rocks from the Saxonian Erzgebirge and the Kokchetav Massif: are so-called diamondiferous gneisses magmatic rocks? Earth Planet. Sci. Lett. 216, 347–364. https://doi.org/10.1016/S0012-821X(03)00512-0

Massonne, H.J., 2005. Involvement of crustal material in delamination of the lithosphere after continent-continent collision. Int. Geol. Rev. 47, 792–804. https://doi.org/10.2747/0020-6814.47.8.792

Massonne, H.J., 2011. German part of the Saxonian Erzgebirge. International Eclogite Conference, 9th, Pre-Conference Excursion: Mariánské Lázně, Czech Republic. Geolines. 23, 29–59.

Massonne, H.J., 2021. Comment to “Deep subduction of felsic rocks hosting UHP lenses in the central Saxonian Erzgebirge: Implications for UHP terrane exhumation” by Schönig et al. (2020). Gondwana Res. 98, 317–319. https://doi.org/10.1016/j.gr.2020.12.028

Massonne, H.J., Schreyer, W., 1987. Phengite geobarometry based on the limiting assemblage with K-feldspar, phlogopite, and quartz. Contrib. Mineral. Petrol. 96, 212–224. https://doi.org/10.1007/BF00375235

Massonne, H.J., Kennedy, A., Nasdala, L., Theye, T., 2007. Dating of zircon and monazite from diamondiferous quartzofeldspathic rocks of the Saxonian Erzgebirge–hints at burial and exhumation velocities. Mineral. Mag. 71, 407–425. https://doi.org/10.1180/minmag.2007.071.4.407

Mazzucchelli, M.L., Burnley, P., Angel, R.J., Morganti, S., Domeneghetti, M.C., Nestola, F., Alvaro, M., 2018. Elastic geothermobarometry: Corrections for the geometry of the host-inclusion system. Geology 46, 231–234. https://doi.org/10.1130/G39807.1

Mazzucchelli, M.L., Angel, R.J., Alvaro, M., 2021. EntraPT: An online platform for elastic geothermobarometry. Am. Mineral. 106, 830–837. https://doi.org/10.2138/am-2021-7693CCBYNCND

McInnes, B.I.A., Evans, N.J., McDonald, B.J., Kinny, P.D., Jakimowicz, J., 2009. Zircon U–Th–Pb–He double dating of the Merlin kimberlite field, northern territory, Australia. Lithos 112, 592–599. https://doi.org/10.1016/j.lithos.2009.05.006

Medaris, L.G., 1980. Convergent metamorphism of eclogite and garnet-bearing ultramafic rocks at Lien, West Norway. Nature 283, 470–472. https://doi.org/10.1038/283470a0

Meinhold, G., Anders, B., Kostopoulos, D., Reischmann, T., 2008. Rutile chemistry and thermometry as provenance indicator: an example from Chios Island, Greece. Sediment. Geol. 203, 98–111. https://doi.org/10.1016/j.sedgeo.2007.11.004

Meinhold, G., 2010. Rutile and its applications in earth sciences. Earth-Sci. Rev. 102, 1–28. https://doi.org/10.1016/j.earscirev.2010.06.001

Millonig L.J., Albert, R., Gerdes, A., Avigad, D., Dietsch, C., 2020. Exploring laser ablation U–Pb dating of regional metamorphic garnet–The Straits Schist, Connecticut, USA. Earth Planet. Sci. Lett. 552, 116589. https://doi.org/10.1016/j.epsl.2020.116589

Mints, M.V., Belousova, E.A., Konilov, A.N., Natapov, L.M., Shchipansky, A.A., Griffin, W.L., O'Reilly, S.Y., Dokukina, K.A., Kaulina, T.V., 2010. Mesoarchean subduction processes: 2.87 Ga eclogites from the Kola Peninsula, Russia. Geology 38, 739–742. https://doi.org/10.1130/G31219.1

Moecher, D.P., Samson, S.D., 2006. Differential zircon fertility of source terranes and natural bias in the detrital zircon record: implications for sedimentary provenance analysis. Earth Planet. Sci. Lett. 247, 252–266. https://doi.org/10.1016/j.epsl.2006.04.035

Möller, A., Appel, P., Mezger, K., Schenk, V., 1995. Evidence for a 2 Ga subduction zone: eclogites in the Usagaran belt of Tanzania. Geology 23, 1067–1070. https://doi.org/10.1130/0091-7613(1995)023<1067:EFAGSZ>2.3.CO;2

Möller, A., O'Brien, P.J., Kennedy, A., Kröner, A., 2002. Polyphase zircon in ultrahigh-temperature granulites (Rogaland, SW Norway): Constraints for Pb diffusion in zircon. J. Metamorph. Geol. 20, 727–740. https://doi.org/10.1046/j.1525-1314.2002.00400.x

Möller, A., O'Brien, P.J., Kennedy, A., Kröner, A., 2003. Linking growth episodes of zircon and metamorphic textures to zircon chemistry: an example from the ultrahigh-temperature granulites of Rogaland (SW Norway). In: Vance, D., Müller, W., Villa, I.M. (Eds.), Geochronology: Linking the Isotopic Record with Petrology and Textures. Geol. Soc. London Spec. Pub. 220, 65–81. https://doi.org/10.1144/GSL.SP.2003.220.01.04

Monteleone, B.D., Baldwin, S.L., Webb, L.E., Fitzgerald, P.G., Grove, M., Schmitt, A.K., 2007. Late Miocene–Pliocene eclogite facies metamorphism, D'Entrecasteaux Islands, SE Papua New Guinea. J. Metamorph. Geol. 25, 245–265. https://doi.org/10.1111/j.1525-1314.2006.00685.x

Morton, A.C., 1985. A new approach to provenance studies: electron microprobe analysis of detrital garnets from Middle Jurassic sandstones of Northern Sea. Sedimentology 32, 553–566. https://doi.org/10.1111/j.1365-3091.1985.tb00470.x

Morton, A.C., Hallsworth, C.R., 1999. Processes controlling the composition of heavy mineral assemblages in sandstones. Sediment. Geol. 124, 3–29. https://doi.org/10.1016/S0037-0738(98)00118-3

Morton, A.C., Whitham, A.G., Fanning, C.M., 2005. Provenance of Late Cretaceous to Paleocene submarine fan sandstones in the Norwegian Sea: integration of heavy mineral, mineral chemical and zircon age data. Sediment. Geol. 182, 3–28. https://doi.org/10.1016/j.sedgeo.2005.08.007

Mosenfelder, J.L., Bohlen S.R., 1997. Kinetics of the coesite to quartz transformation. Earth Planet. Sci. Lett. 153, 133–147. https://doi.org/10.1016/S0012-821X(97)00159-3

Mosenfelder, J.L., Schertl, H.-P., Smyth, J.R., Liou, J.G., 2005. Factors in the preservation of coesite: The importance of fluid infiltration. Am. Mineral. 90, 779–789. https://doi.org/10.2138/am.2005.1687

Müller, S., Dziggel, A., Kolb, J., Sindern, S., 2018a. Mineral textural evolution and PT-path of relict eclogite-facies rocks in the Paleoproterozoic Nagssugtoqidian Orogen, South-East Greenland. Lithos 296, 212–232. https://doi.org/10.1016/j.lithos.2017.11.008

Müller, S., Dziggel, A., Sindern, S., Kokfelt, T.F., Gerdes, A., Kolb, J., 2018b. Age and temperature-time evolution of retrogressed eclogite-facies rocks in the Paleoproterozoic Nagssugtoqidian Orogen, South-East Greenland: Constrained from U-Pb dating of zircon, monazite, titanite and rutile. Precambrian Res. 314, 468–486. https://doi.org/10.1016/j.precamres.2018.07.002

Murri, M., Mazzucchelli, M.L., Campomenosi, N., Korsakov, A.V., Prencipe, M., Mihailova, B.D., Scambelluri, M., Angel, R., Alvaro, M., 2018. Raman elastic geobarometry for anisotropic mineral inclusions. Am. Mineral. 103, 1869–1872. https://doi.org/10.2138/am-2018-6625CCBY

Nasdala, L., Massonne, H.J., 2000. Microdiamonds from the Saxonian Erzgebirge, Germany: in situ micro-Raman characterization. Eur. J. Mineral. 12, 495–498. https://doi.org/10.1127/0935-1221/2000/0001-0495

Nie, S., Yin, A., Rowley, D.B., Jin, Y., 1994. Exhumation of the Dabie Shan ultra-high-pressure rocks and accumulation of the Songpan-Ganzi flysch sequence, central China. Geology 22, 999–1002. https://doi.org/10.1130/0091-7613(1994)022<0999:EOTDSU>2.3.CO;2

Nowicki, T.E., Moore, R.O., Gurney, J.J., Baumgartner, M.C., 2007. Diamonds and associated heavy minerals in kimberlite: a review of key concepts and applications. In: Mange, M.A., Wright, D.T. (Eds.), Dev. Sedimentol. 58, 1235–1267. https://doi.org/10.1016/S0070-4571(07)58046-5

Nutman, A.P., Friend, C.R., Bennett, V.C., 2002. Evidence for 3650–3600 Ma assembly of the northern end of the Itsaq Gneiss Complex, Greenland: implication for early Archaean tectonics. Tectonics 21, TC001203. https://doi.org/10.1029/2000TC001203

Nutman, A.P., Bennett, V.C., Friend, C.R., Yi, K., 2020. Eoarchean contrasting ultra-high-pressure to low-pressure metamorphisms (<250 to >1000°C/GPa) explained by tectonic plate convergence in deep time. Precambrian Res. 344, 105770. https://doi.org/10.1016/j.precamres.2020.105770

Ogasawara, Y., Fukasawa, K., Maruyama, S., 2002. Coesite exsolution from supersilicic titanite in UHP marble from the Kokchetav Massif, northern Kazakhstan. Am. Mineral. 87, 454–461. https://doi.org/10.2138/am-2002-0409

O'Neill, C., Turner, S., Rushmer, T., 2018. The inception of plate tectonics: a record of failure. Philos. Trans. Royal Soc. A 376, 20170414. https://doi.org/10.1098/rsta.2017.0414

Osborne, Z.R., Thomas, J.B., Nachlas, W.O., Baldwin, S.L., Holycross, M.E., Spear, F.S., Watson, E.B., 2019. An experimentally calibrated thermobarometric solubility model for titanium in coesite (TitaniC). Contrib. Mineral. Petrol. 174, 1–13. https://doi.org/10.1007/s00410-019-1575-5

Ota, T., Kobayashi, K., Kunihiro, T., Nakamura, E., 2008. Boron cycling by subducted lithosphere; insights from diamondiferous tourmaline from the Kokchetav ultrahigh-pressure metamorphic belt. Geochim. Cosmochim. Acta 72, 3531–3541. https://doi.org/10.1016/j.gca.2008.05.002

Palin, R.M., Santosh, M., Cao, W., Li, S.S., Hernández-Uribe, D., Parsons, A., 2020. Secular change and the onset of plate tectonics on Earth. Earth-Sci. Rev. 207, 103172. https://doi.org/10.1016/j.earscirev.2020.103172

Parkinson, C.D., Katayama, I., 1999. Present-day ultrahigh-pressure conditions of coesite inclusions in zircon and garnet: Evidence from laser Raman microspectroscopy. Geology 27, 979–982. https://doi.org/10.1130/0091-7613(1999)027<0979:PDUPCO>2.3.CO;2

Pease, V., Percival, J., Smithies, H., Stevens, G., van Kranendonk, M., 2008. When did plate tectonics begin? Evidence from the orogenic record. In: Condie, K.C., Pease, V. (Eds.), When did plate tectonics begin on planet Earth? GSA Special Paper 440, 199–228.

Peltonen, P., Kontinen, A., Huhma, H., 1996. Petrology and geochemistry of metabasalts from the 1.95 Ga Jormua ophiolite, northeastern Finland. J. Petrol. 37, 1359–1383. https://doi.org/10.1093/petrology/37.6.1359

Perchuk, A.L., Morgunova, A.A., 2014. Variable P–T paths and HP-UHP metamorphism in a Precambrian terrane, Gridino, Russia: Petrological evidence and geodynamic implications. Gondwana Res. 25, 614–629. https://doi.org/10.1016/j.gr.2012.09.009

Pereira, I., Storey, C.D., Darling, J.R., Lana, C., Alkmim, A.R., 2019. Two billion years of evolution enclosed in hydrothermal rutile: recycling of the São Francisco Craton Crust and constraints on gold remobilisation processes. Gondwana Res. 68, 69–92. https://doi.org/10.1016/j.gr.2018.11.008

Pidgeon, R.T., 1992. Recrystallisation of oscillatory zoned zircon: some geochronological and petrological implications. Contrib. Mineral. Petrol. 110, 463–472. https://doi.org/10.1007/BF00344081

Prencipe, M., 2012. Simulation of vibrational spectra of crystals by ab initio calculations: an invaluable aid in the assignment and interpretation of the Raman signals. The case of jadeite ($NaAlSi_2O_6$). J. Raman Spectrosc. 43, 1567–1569. https://doi.org/10.1002/jrs.4040

Rahl, J.M., Reiners, P.W., Campbell, I.H., Nicolescu, S., Allen, C.M., 2003. Combined single-grain (U–Th)/He and U/Pb dating of detrital zircons from the Navajo Sandstone, Utah. Geology 31, 761–764. https://doi.org/10.1130/G19653.1

Reimink, J.R., Davies, J.H.F.L., Ielpi, A., 2021. Global zircon analysis records a gradual rise of continental crust throughout the Neoarchean. Earth Planet. Sci. Lett. 554, 116654. https://doi.org/10.1016/j.epsl.2020.116654

Reinecke, T., 1991. Very-high-pressure metamorphism and uplift of coesite-bearing metasediments from the Zermatt-Saas zone, Western Alps. Eur. J. Mineral. 3, 7–18. https://doi.org/10.1127/ejm/3/1/0007

Reiners, P.W., 2005. Zircon (U–Th)/He thermochronometry. Rev. Mineral. Geochem. 58, 151–179. https://doi.org/10.2138/rmg.2005.58.6

Reiners, P., Campbell, I.H., Nicolescu, S., Allen, C.M., Garver, J.I., Hourigan, J.K., Cowan, D.S., 2004. Double-and triple-dating of single detrital zircons with (U–Th)/He, fission-track, and U/Pb systems, and examples from modern and ancient sediments of the western US. American Geophysical Union, Fall Meeting 2004, Abstract T51D-01.

Reiners, P.W., Campbell, I.H., Nicolescu, S., Allen, C.M., Hourigan, J.K., Garver, J.I., Mattinson, J.M., Cowan, D.S., 2005. (U-Th)/(He-Pb) double dating of detrital zircons. Am. J. Sci. 305, 259–311. https://doi.org/10.2475/ajs.305.4.259

Reverdatto, V.V., Likhanov, I.I., Polyansky, O.P., Sheplev, V.S., Kolobov, V.Y., 2019. Mineral Geothermobarometry. In: Reverdatto, V.V., Likhanov, I.I., Polyansky, O.P., Sheplev, V.S., Kolobov, V.Y. (Eds), The Nature and Models of Metamorphism. Springer Nature Switzerland, Cham, 55–82. https://doi.org/10.1007/978-3-030-03029-2_2.

Rezvukhina, O.V., Skublov, S.G., Rezvukhin, D.I., Korsakov, A.V., 2021. Rutile in diamondiferous metamorphic rocks: New insights from trace-element composition, mineral/fluid inclusions, and U-Pb ID-TIMS dating. Lithos 394, 106172. https://doi.org/10.1016/j.lithos.2021.106172

Robinson, P.T., Bai, W.J., Malpas, J., Yang, J.S., Zhou, M.F., Fang, Q., Hu, X.F.S., Cameron, S., Staudigel, H., 2004. Ultrahigh-pressure minerals in the Luobusa Ophiolite, Tibet, and their tectonic implications. In: Malpas, J., Fletcher, C.J.N., Ali, J.R., Aitchison, J.C. (Eds.), Aspects of the Tectonic Evolution of China. Geol. Soc. London Spec. Publ. 226, 247–271. https://doi.org/10.1144/GSL.SP.2004.226.01.14

Root, D.B., Hacker, B.R., Gans, P.B., Ducea, M.N., Eide, E.A., Mosenfelder, J.L., 2005. Discrete ultrahigh-pressure domains in the Western Gneiss Region, Norway: implications for formation and exhumation. J. Metamorph. Geol. 23, 45–61. https://doi.org/10.1111/j.1525-1314.2005.00561.x

Rubatto, D., 2002. Zircon trace element geochemistry: partitioning with garnet and the link between U–Pb ages and metamorphism. Chem. Geol. 184, 123–138. https://doi.org/10.1016/S0009-2541(01)00355-2

Rubatto, D., 2017. Zircon: the metamorphic mineral. Rev. Mineral. Geochem. 83, 261–295. https://doi.org/10.2138/rmg.2017.83.9

Rubatto, D., Gebauer, D., 2000. Use of cathodoluminescence for U-Pb zircon dating by ion microprobe: some examples from the Western Alps. In: Pagel, M., Barbin, V., Blanc, P., Ohnenstetter, D. (Eds.), Cathodoluminescence in Geosciences. Springer, Berlin, Heidelberg, 373–400. https://doi.org/10.1007/978-3-662-04086-7_15

Rubatto, D., Müntener, O., Barnhoorn, A., Gregory, C., 2008. Dissolution-reprecipitation of zircon at low-temperature, high-pressure conditions (Lanzo Massif, Italy). Am. Mineral. 93, 1519–1529.

Satkoski, A.M., Fralick, P., Beard, B.L., Johnson, C.M., 2017. Initiation of modern-style plate tectonics recorded in Mesoarchean marine chemical sediments. Geochim. Cosmochim. Acta 209, 216–232. https://doi.org/10.1016/j.gca.2017.04.024

Schertl, H.P., Hertwig, A., Maresch, W.V., 2019. Cathodoluminescence microscopy of zircon in HP- and UHP-metamorphic rocks: A fundamental technique for assessing the problem of inclusions

versus pseudo-inclusions. J. Earth Sci. 30, 1095–1107. https://doi.org/10.1007/s12583-019-1246-5

Schmädicke, E., Okrusch, M., Schmidt, W., 1992. Eclogite-facies rocks in the Saxonian Erzgebirge, Germany: high pressure metamorphism under contrasting *P–T* conditions. Contrib. Mineral. Petrol. 110, 226–241. https://doi.org/10.1007/BF00310740

Schönig, J., Meinhold, G., von Eynatten, H., Lünsdorf, N.K., 2018a. Tracing ultrahigh pressure metamorphism at the catchment scale. Sci. Rep. 8, 2931. https://doi.org/10.1038/s41598-018-21262-8

Schönig, J., Meinhold, G., von Eynatten, H., Lünsdorf, N.K., 2018b. Provenance information recorded by mineral inclusions in detrital garnet. Sediment. Geol. 376, 32–49. https://doi.org/10.1016/j.sedgeo.2018.07.009

Schönig, J., von Eynatten, H., Meinhold, G., Lünsdorf, N.K., 2019. Diamond and coesite inclusions in detrital garnet of the Saxonian Erzgebirge, Germany. Geology 47, 715–718. https://doi.org/10.1130/G46253.1

Schönig, J., von Eynatten, H., Meinhold, G., Lünsdorf, N.K., Willner, A.P., Schulz, B., 2020. Deep subduction of felsic rocks hosting UHP lenses in the central Saxonian Erzgebirge: Implications for UHP terrane exhumation. Gondwana Res. 87, 320–329. https://doi.org/10.1016/j.gr.2020.06.020

Schönig, J., von Eynatten, H., Tolosana-Delgado, R., Meinhold, G., 2021a. Garnet major-element composition as an indicator of host-rock type: a machine learning approach using the random forest classifier. Contrib. Mineral. Petrol. 176, 98. https://doi.org/10.1007/s00410-021-01854-w

Schönig, J., von Eynatten, H., Meinhold, G., Lünsdorf, N.K., 2021b. Life-cycle analysis of coesite-bearing garnet. Geol. Mag. 158, 1421–1440. https://doi.org/10.1017/S0016756821000017

Schönig, J., von Eynatten, H., Meinhold, G., Lünsdorf, N.K., Willner, A.P., Schulz, B., 2021c. Reply to comment on “Deep subduction of felsic rocks hosting UHP lenses in the central Saxonian Erzgebirge: Implications for UHP terrane exhumation”. Gondwana Res. 98, 320–323. https://doi.org/10.1016/j.gr.2020.12.029

Schulze, D.J., 2003. A classification scheme for mantle-derived garnets in kimberlite: a tool for investigating the mantle and exploring for diamonds. Lithos 71, 195–213. https://doi.org/10.1016/S0024-4937(03)00113-0

Schulze, D.J., Valley, J.W., Spicuzza, M.J., 2000. Coesite eclogites from the Roberts Victor kimberlite, South Africa. Lithos 54, 23–32. https://doi.org/10.1016/S0024-4937(00)00031-1

Scott, D.J., Helmstaedt, H., Bickle, M.J., 1992. Purtuniq ophiolite, Cape Smith belt, northern Quebec, Canada: A reconstructed section of Early Proterozoic oceanic crust. Geology 20, 173–176. https://doi.org/10.1130/0091-7613(1992)020<0173:POCSBN>2.3.CO;2

Shatsky, V.S., Sobolev, N.V., 1993. Some specific features of the origin of diamonds in metamorphic rocks. Dokl. Akad. Nauk 331, 217–219.

Shirey, S.B., Richardson, S.H., 2011. Start of the Wilson cycle at 3 Ga shown by diamonds from subcontinental mantle. Science 333, 434–436. https://doi.org/10.1126/science.1206275

Shirey, S.B., Kamber, B.S., Whitehouse, M.J., Mueller, P.A., Basu, A.R., 2008. A review of the isotopic and trace element evidence for mantle and crustal processes. In: Condie, K.C., Pease, V. (Eds.), When did plate tectonics begin on planet Earth? GSA Spec. Pap. 440, 1–29.

Sizova, E., Gerya, T., Brown, M., Perchuk, L.L., 2010. Subduction styles in the Precambrian: Insight from numerical experiments. Lithos 116, 209–229. https://doi.org/10.1016/j.lithos.2009.05.028

Sizova, E., Gerya, T., Brown, M., 2014. Contrasting styles of Phanerozoic and Precambrian continental collision. Gondwana Res. 25, 522–545. https://doi.org/10.1016/j.gr.2012.12.011

Smith, D.C., 1984. Coesite in clinopyroxene in the Caledonides and its implications for geodynamics. Nature 310, 641–644. https://doi.org/10.1038/310641a0

Smyth, J.R., Hatton, C.J., 1977. A coesite-sanidine grospydite from the Roberts Victor kimberlite. Earth Planet. Sci. Lett. 34, 284–290. https://doi.org/10.1016/0012-821X(77)90012-7

Smythe, D.J., Schulze, D.J., Brenan, J.M., 2008. Rutile as a kimberlite indicator mineral: minor and trace element geochemistry. 9th International Kimberlite Conference, Extended Abstract, No. 9IKC-A-00193

Sobolev, N.V., Shatsky, V.S., 1990. Diamond inclusions in garnets from metamorphic rocks: a new environment for diamond formation. Nature 343, 742–745. https://doi.org/10.1038/343742a0

Spear, F.S., Wolfe, O.M., 2020. Revaluation of “equilibrium” PT paths from zoned garnet in light of quartz inclusion in garnet (QuiG) barometry. Lithos 372, 105650. https://doi.org/10.1016/j.lithos.2020.105650

Spencer, C.J., Roberts, N.M.W., Santosh, M., 2017. Growth, destruction, and preservation of Earth's continental crust. Earth-Sci. Rev. 172, 87–106. https://doi.org/10.1016/j.earscirev.2017.07.013

Spengler, D., van Roermund, H.L., Drury, M.R., Ottolini, L., Mason, P.R., Davies, G.R., 2006. Deep origin and hot melting of an Archaean orogenic peridotite massif in Norway. Nature 440, 913–917. https://doi.org/10.1038/nature04644

Stepanov, A.S., Hermann, J., Rubatto, D., Rapp, R.P., 2012. Experimental study of monazite/melt partitioning with implications for the REE, Th and U geochemistry of crustal rocks. Chem. Geol. 300, 200–220. https://doi.org/10.1016/j.chemgeo.2012.01.007

Stepanov, A.S., Hermann, J., Korsakov, A.V., Rubatto, D., 2014. Geochemistry of ultrahigh-pressure anatexis: fractionation of elements in the Kokchetav gneisses during melting at diamond-facies conditions. Contrib. Mineral. Petrol. 167, 1002. 10.1007/s00410-014-1002-x

Stepanov, A.S., Rubatto, D., Hermann, J., Korsakov, A.V., 2016. Contrasting PT paths within the Barchi-Kol UHP terrain (Kokchetav Complex): Implications for subduction and exhumation of continental crust. Am. Mineral. 101, 788–807. https://doi.org/10.2138/am-2016-5454

Stern, R.J., 2005. Evidence from ophiolites, blueschists, and ultrahigh-pressure metamorphic terranes that the modern episode of subduction tectonics began in Neoproterozoic time. Geology 33, 557–560. https://doi.org/10.1130/G21365.1

Stern, R.J., 2018. The evolution of plate tectonics. In: Hawkesworth, C., Brown. M. (Eds.), Earth dynamics and the development of plate tectonics. Philos. Trans. Royal Soc. A 376, 20170406. https://doi.org/10.1098/rsta.2017.0406

Stern, R.J., Leybourne, M.I., Tsujimori, T., 2016. Kimberlites and the start of plate tectonics. Geology 44, 799–802. https://doi.org/10.1130/G38024.1

Tang, M., Chen, K., Rudnick, R.L., 2016. Archean upper crust transition from mafic to felsic marks the onset of plate tectonics. Science 351, 372–375. https://doi.org/10.1126/science.aad5513

Tang, M., Ji, W.Q., Chu, X., Wu, A., Chen, C., 2021a. Reconstructing crustal thickness evolution from europium anomalies in detrital zircons. Geology 49, 76–80. https://doi.org/10.1130/G47745.1

Tang, M., Chu, X., Hao, J., Shen, B., 2021b. Orogenic quiescence in Earth's middle age. Science 371, 728–731. https://doi.org/10.1126/science.abf1876

Taguchi, T., Igami, Y., Miyake, A., Masaki, E., 2019. Factors affecting preservation of coesite in ultrahigh-pressure metamorphic rocks: Insights from TEM observations of dislocations within kyanite. J. Metamorph. Geol. 37, 401–414. https://doi.org/10.1111/jmg.12470

Taguchi, T., Kouketsu, Y., Igami, Y., Kobayashi, T., Miyake, A., 2021. Hidden intact coesite in deeply subducted rocks. Earth Planet. Sci. Lett. 558, 116763. https://doi.org/10.1016/j.epsl.2021.116763

Teraoka, Y., Suzuki, M., Kawakami, K., 1998. Provenance of Cretaceous and Paleogene sediments in the median zone of Southwest Japan. Bull. Geol. Surv. Japan 49, 395–411.

Thiessen, E.J., Gibson, H.D., Regis, D., Pehrsson, S.J., Cutts, J.A., Smit, M.A., 2019. High-grade metamorphism flying under the radar of accessory minerals. Geology 47, 568–572. https://doi.org/10.1130/G45979.1

Tichomirowa, M., Whitehouse, M., Gerdes, A., Schulz, B., 2018. Zircon (Hf, O isotopes) as melt indicator: Melt infiltration and abundant new zircon growth within melt rich layers of granulite-facies lenses versus solid-state recrystallization in hosting amphibolite-facies gneisses (central Erzgebirge, Bohemian Massif). Lithos 302, 65–85. https://doi.org/10.1016/j.lithos.2017.12.020

Tolosana-Delgado, R., von Eynatten, H., Krippner, A., Meinhold, G., 2018. A multivariate discrimination scheme of detrital garnet chemistry for use in sedimentary provenance analysis. Sediment. Geol. 375, 14–26. https://doi.org/10.1016/j.sedgeo.2017.11.003

Tomaschek, F., Kennedy, A.K., Villa, I.M., Lagos, M., Ballhaus, C., 2003. Zircons from Syros, Cyclades, Greece—recrystallization and mobilization of zircon during high-pressure metamorphism. J. Petrol. 44, 1977–2002. https://doi.org/10.1093/petrology/egg067

Tomkins, H.S., Powell, R., Ellis, D.J., 2007. The pressure dependence of the zirconium-in-rutile thermometer. J. Metamorph. Geol. 25, 703–713. https://doi.org/10.1111/j.1525-1314.2007.00724.x

Toth, J., Gurnis, M., 1998. Dynamics of subduction initiation at preexisting fault zones. J. Geophys. Res. Solid Earth 103, 18053–18067. https://doi.org/10.1029/98JB01076

Triebold, S., von Eynatten, H., Luvizotto, G.L., Zack, T., 2007. Deducing source rock lithology from detrital rutile geochemistry: an example from the Erzgebirge, Germany. Chem. Geol. 244, 421–436. https://doi.org/10.1016/j.chemgeo.2007.06.033

Triebold, S., von Eynatten, H., Zack, T., 2012. A recipe for the use of rutile in sedimentary provenance analysis. Sediment. Geol. 282, 268–275. https://doi.org/10.1016/j.sedgeo.2012.09.008

Trumbull, R.B., Krienitz, M.S., Grundmann, G., Wiedenbeck, M., 2009. Tourmaline geochemistry and $\delta^{11}B$ variations as a guide to fluid–rock interaction in the Habachtal emerald deposit, Tauern Window, Austria. Contrib. Mineral. Petrol. 157, 411–427. https://doi.org/10.1007/s00410-008-0342-9

Ueda, K., Gerya, T., Sobolev, S.V., 2008. Subduction initiation by thermal–chemical plumes: numerical studies. Phys. Earth Planet. Inter. 171, 296–312. https://doi.org/10.1016/j.pepi.2008.06.032

Usui, T., Kobayashi, K., Nakamura, E., 2002. U–Pb isotope systematics of micro-zircon inclusions: Implications for the age and origin of eclogite xenolith from the Colorado Plateau. Proc. Jpn. Acad. 78, 51–56. https://doi.org/10.2183/pjab.78.51

Vavra, G., Gebauer, D., Schmid, R., Compston, W., 1996. Multiple zircon growth and recrystallization during polyphase Late Carboniferous to Triassic metamorphism in granulites of the Ivrea Zone (Southern Alps): an ion microprobe (SHRIMP) study. Contrib. Mineral. Petrol. 122, 337–358. https://doi.org/10.1007/s004100050132

Vavra, G., Schmid, R., Gebauer, D., 1999. Internal morphology, habit and U-Th-Pb microanalysis of amphibolite-to-granulite facies zircons: geochronology of the Ivrea Zone (Southern Alps). Contrib. Mineral. Petrol. 134, 380–404. https://doi.org/10.1007/s004100050492

Venables, W.N., Ripley, B.D., 2002. Modern Applied Statistics with S. Springer-Verlag, New York. https://doi.org/10.1007/978-0-387-21706-2

Vishnevsky, S., Raitala, J., 2000. Impact diamonds as indicators of shock metamorphism in strongly-reworked Pre-Cambrian impactites. In: Gilmour, I., Koeberl, C. (Eds.), Impacts and the Early Earth. Lecture Notes in Earth Sciences 91. Springer, Berlin, Heidelberg. https://doi.org/10.1007/BFb0027762

von Eynatten, H., Gaupp, R., 1999. Provenance of Cretaceous synorogenic sandstones in the Eastern Alps: constraints from framework petrography, heavy mineral analysis, and mineral chemistry. Sediment. Geol. 124, 81–111. https://doi.org/10.1016/S0037-0738(98)00122-5

von Eynatten, H., Dunkl, I., 2012. Assessing the sediment factory: the role of single grain analysis. Earth-Sci. Rev. 115, 97–120. https://doi.org/10.1016/j.earscirev.2012.08.001

von Eynatten, H., Gaupp, R., Wijbrans, J.R., 1996. $^{40}Ar/^{39}Ar$ laser-probe dating of detrital white micas from Cretaceous sedimentary rocks of the Eastern Alps: evidence for Variscan high-pressure metamorphism and implications for Alpine orogeny. Geology 24, 691–694. https://doi.org/10.1130/0091-7613(1996)024<0691:AALPDO>2.3.CO;2

Vry, J.K., Baker, J.A., 2006. LA-MC-ICPMS Pb–Pb dating of rutile from slowly cooled granulites: confirmation of the high closure temperature for Pb diffusion in rutile. Geochim. Cosmochim. Acta 70, 1807–1820. https://doi.org/10.1016/j.gca.2005.12.006

Wan, Y., Li, R., Wilde, S.A., Liu, D., Chen, Z., Yan, L., Song, T., Yin, X., 2005. UHP metamorphism and exhumation of the Dabie Orogen, China: evidence from SHRIMP dating of zircon and monazite from a UHP granitic gneiss cobble from the Hefei Basin. Geochim. Cosmochim. Acta 69, 4333–4348. https://doi.org/10.1016/j.gca.2005.03.055

Wang, C.Y., Campbell, I.H., Reiners, P.W., Allen, C.M., 2014. Detrital zircon U-Pb-He double dating: A method of quantifying long-and short-term exhumation rates in collisional orogens. Sci. China Earth Sci. 57, 2702–2711. https://doi.org/0.1007/s11430-014-4970-9

Wang, L., Wang, S.J., Brown, M., Zhang, J.F., Feng, P., Jin, Z.M., 2018. On the survival of intergranular coesite in UHP eclogite. J. Metamorph. Geol. 36, 173–194. https://doi.org/10.1111/jmg.12288

Watson, E.B., Harrison, T.M., 2005. Zircon thermometer reveals minimum melting conditions on earliest Earth. Science 308, 841–844. https://doi.org/10.1126/science.1110873

Watson, E., Wark, D., Thomas, J., 2006. Crystallization thermometers for zircon and rutile. Contrib. Mineral. Petrol. 151, 413–433. https://doi.org/10.1007/s00410-006-0068-5

Wei, C.J., Clarke, G.L., 2011. Calculated phase equilibria for MORB compositions: a reappraisal of the metamorphic evolution of lawsonite eclogite. J. Metamorph. Geol. 29, 939–952. https://doi.org/10.1111/j.1525-1314.2011.00948.x

Weislogel, A.L., Graham, S.A., Chang, E.Z., Wooden, J.L., Gehrels, G.E., Yang, H., 2006. Detrital zircon provenance of the Late Triassic Songpan-Ganzi complex: Sedimentary record of collision of the North and South China blocks. Geology 34, 97–100. https://doi.org/10.1130/G21929.1

Weislogel, A.L., Graham, S.A., Chang, E.Z., Wooden, J.L., Gehrels, G.E., 2010. Detrital zircon provenance from three turbidite depocenters of the Middle–Upper Triassic Songpan-Ganzi complex, central China: Record of collisional tectonics, erosional exhumation, and sediment production. GSA Bulletin 122, 2041–2062. https://doi.org/10.1130/B26606.1

Weller, O.M., St-Onge, M.R., 2017. Record of modern-style plate tectonics in the Palaeoproterozoic Trans-Hudson orogen. Nat. Geosci. 10, 305–311. https://doi.org/10.1038/ngeo2904

Whitney, D.L., Cooke, M.L., Du Frane, S.A., 2000. Modeling of radial microcracks at corners of inclusions in garnet using fracture mechanics. J. Geophys. Res. 105, 2843–2853. https://doi.org/10.1029/1999JB900375

Willner, A.P., Rötzler, K., Maresch, W.V., 1997. Pressure-temperature and fluid evolution of quartzo-feldspathic metamorphic rocks with a relic high-pressure, granulite-facies history from the Central Erzgebirge (Saxony, Germany). J. Petrol. 38, 307–336. https://doi.org/10.1093/petroj/38.3.307

Wright, W.I., 1938. The composition and occurrence of garnets. Am. Mineral. 23, 436–449.

Xie, S., Wu, Y., Zhang, Z., Qin, Y., Liu, X., Wang, H., Qin, Z., Liu, Q., Yang, S., 2012. U–Pb ages and trace elements of detrital zircons from Early Cretaceous sedimentary rocks in the Jiaolai Basin, north margin of the Sulu UHP terrane: Provenances and tectonic implications. Lithos 154, 346–360. https://doi.org/10.1016/j.lithos.2012.08.002

Xu, C., Kynický, J., Song, W., Tao, R., Lü, Z., Li, Y., Yang, Y., Pohanka, M., Galiova, M.V., Zhang, L., Fei, Y., 2018. Cold deep subduction recorded by remnants of a Paleoproterozoic carbonated slab. Nat. Commun. 9, 2790. https://doi.org/10.1038/s41467-018-05140-5

Yakymchuk, C., Kirkland, C.L., Clark, C., 2018. Th/U ratios in metamorphic zircon. J. Metamorph. Geol. 36, 715–737. https://doi.org/10.1111/jmg.12307

Yamamoto, S., Komiya, T., Hirose, K., Maruyama, S., 2009. Coesite and clinopyroxene exsolution lamellae in chromites: In-situ ultrahigh-pressure evidence from podiform chromitites in the Luobusa ophiolite, southern Tibet. Lithos 109, 314–322. https://doi.org/10.1016/j.lithos.2008.05.003

Ye, K., Yao, Y., Katayama, I., Cong, B., Wang, Q., Maruyama, S., 2000. Large areal extent of ultrahigh-pressure metamorphism in the Sulu ultrahigh-pressure terrane of East China: new implications from coesite and omphacite inclusions in zircon of granitic gneiss. Lithos 52, 157–164. https://doi.org/10.1016/S0024-4937(99)00089-4

Yong, W., Dachs, E., Benisek, A., Secco, R.A., 2012. Heat capacity, entropy and phase equilibria of stishovite. Phys. Chem. Miner. 39, 153–162. https://doi.org/10.1007/s00269-011-0470-z

Zack, T., Kooijman, E., 2017. Petrology and geochronology of rutile. Rev. Mineral. Geochem. 83, 443–467. https://doi.org/10.2138/rmg.2017.83.14

Zack, T., von Eynatten, H., Kronz, A., 2004a. Rutile geochemistry and its potential use in quantitative provenance studies. Sediment. Geol. 171, 37–58. https://doi.org/10.1016/j.sedgeo.2004.05.009

Zack, T., Moraes, R., Kronz, A., 2004b. Temperature dependence of Zr in rutile: empirical calibration of a rutile thermometer. Contrib. Mineral. Petrol. 148, 471–488. https://doi.org/10.1007/s00410-004-0617-8

Zack, T., Stockli, D.F., Luvizotto, G.L., Barth, M.G., Belousova, E., Wolfe, M.R., Hinton, R.W., 2011. In situ U–Pb rutile dating by LA-ICP-MS: ^{208}Pb correction and prospects for geological applications. Contrib. Mineral. Petrol. 162, 515–530. https://doi.org/10.1007/s00410-011-0609-4

Zhang, R.Y., Liou, J.G., 1996. Coesite inclusions in dolomite from eclogite in the southern Dabie Mountains, China: the significance of carbonate minerals in UHPM rocks. Am. Mineral. 81, 181–186. https://doi.org/10.2138/am-1996-1-222

Zhang, L., Wang, Y., 2020. The exhumation of high-and ultrahigh-pressure metamorphic terranes in subduction zone: Questions and discussions. Sci. China Earth Sci. 63, 1884–1903. https://doi.org/10.1007/s11430-020-9579-3

Zhang, R.Y., Hirajima, T., Banno, S., Cong, B., Liou, J.G., 1995. Petrology of ultrahigh-pressure rocks from the southern Su-Lu region, eastern China. J. Metamorph. Geol. 13, 659–675. https://doi.org/10.1111/j.1525-1314.1995.tb00250.x

Zhang, K.J., Li, B., Wei, Q.G., Cai, J.X., Zhang, Y.X., 2008. Proximal provenance of the western Songpan–Ganzi turbidite complex (Late Triassic, eastern Tibetan plateau): Implications for the tectonic amalgamation of China. Sediment. Geol. 208, 36–44. https://doi.org/10.1016/j.sedgeo.2008.04.008

Zhang, Z.M., Schertl, H.P., Wang, J.L., Shen, K., Liou, J.G., 2009. Source of coesite inclusions within inherited magmatic zircon from Sulu UHP rocks, eastern China, and their bearing for fluid–rock interaction and SHRIMP dating. J. Metamorph. Geol. 27, 317–333. https://doi.org/10.1111/j.1525-1314.2009.00819.x

Zhang, K.J., Li, B. and Wei, Q.G., 2012. Diversified provenance of the Songpan-Ganzi Triassic turbidites, central China: constraints from geochemistry and Nd isotopes. J. Geol. 120, 69–82. https://doi.org/10.1086/662716

Zhong, X., Andersen, N.H., Dabrowski, M., Jamtveit, B., 2019. Zircon and quartz inclusions in garnet used for complementary Raman thermobarometry: application to the Holsnøy eclogite, Bergen Arcs, Western Norway. Contrib. Mineral. Petrol. 174, 50. https://doi.org/10.1007/s00410-019-1584-4

Zhou, T., Li, Q., Klemd, R., Shi, Y., Tang, X., Li, C., Liu, Y., 2020. Multi-system geochronology of North Dabie eclogite: Ineffective garnet ‘shielding’ on rutile inclusions under multi-thermal conditions. Lithos 368, 105573. https://doi.org/10.1016/j.lithos.2020.105573

Zhukov, V.P., Korsakov, A.V., 2015. Evolution of host-inclusion systems: a visco-elastic model. J. Metamorph. Geol. 33, 815–828. https://doi.org/10.1111/jmg.12149

Zicovich-Wilson, C.M., Pascale, F., Roetti, C., Saunders, V.R., Orlando, R., Dovesi, R., 2004. Calculation of the vibration frequencies of α-quartz: The effect of Hamiltonian and basis set. J. Comput. Chem. 25, 1873–1881. https://doi.org/10.1002/jcc.20120

Figure captions

Figure 1. Global map showing locations where detrital approaches have been applied to trace the erosion of UHP rocks. (A) Qinling–Dabie–Sulu Orogen (China) modified from Zhang et al. (2012); (B) Western Gneiss Region (Norway) modified from Root et al. (2005); Krippner et al. (2016), and Schönig et al. (2018a); (C) Saxonian Erzgebirge (Germany) modified from Linnemann et al. (2012) and Schönig et al. (2020); and (D) D'Entrecasteaux metamorphic complex (Papua New Guinea) modified from Baldwin et al. (2021).

Figure 2. Photomicrographs and Raman images of UHP inclusions in detrital garnet. (A) Monomineralic coesite inclusions. (B) Coesite inclusions partially transformed to quartz. (C) Diamond inclusions. White pixels correspond to inhomogeneities or unidentified phases. Parts are modified from Schönig et al. (2018a) for the Western Gneiss Region in Norway, from Schönig et al. (2019, 2020, 2021b) for the Saxonian Erzgebirge in Germany, and Baldwin et al. (2021) for the D'Entrecasteaux metamorphic complex in Papua New Guinea.

Figure 3: Discrimination scheme classification for crustal *vs.* mantle origin of coesite- and diamond-bearing detrital garnet. (A) Graphical discrimination scheme of Hardman et al. (2018) for mean compositions of individual garnet grains. (B) Mean votes for 'setting' classes of individual garnet grains using the 'setting and metamorphic facies' model of Schönig et al. (2021a). IG – igneous; MS – metasomatic; MM – metamorphic; and MA – mantle. Garnet compositions of the Western Gneiss Region in Norway from Schönig et al. (2018a), of the Saxonian Erzgebirge in Germany from Schönig

et al. (2019, 2020), and the D'Entrecasteaux metamorphic complex in Papua New Guinea from Baldwin et al. (2021).

Figure 4: Comparison of detrital UHP garnet composition with regard to source-rock composition. (A) Mean votes for 'composition' classes of individual UHP garnet grains after Schönig et al. (2021a). IF/S – intermediate–felsic/metasedimentary; CS – calcsilicate; M – mafic; and UM – ultramafic. (B) Comparison of detrital UHP garnet mean composition and inclusion-assemblage with garnet from local crystalline rocks in the X_{Fe+Mn}–X_{Mg}–X_{Ca} ternary diagram (molar proportions). Garnet compositions and inclusion assemblages of the Western Gneiss Region in Norway from Schönig et al. (2018a), of the Saxonian Erzgebirge in Germany from Schönig et al. (2019, 2020, 2021b), and the D'Entrecasteaux metamorphic complex in Papua New Guinea from Baldwin et al. (2021). Crystalline and detrital graphite- and omphacite-bearing garnet compositions shown as kernel density estimate maps, with bandwidths calculated after Venables and Ripley (2002).

Figure 5: Prediction of metamorphic host-rock facies based on major-element composition of detrital coesite- and diamond-bearing garnet grains. (A) Discrimination according to mean probabilities after Tolosana-Delgado et al. (2018) using prior 'equal-M'. EC – eclogite facies; GR – granulite facies; and AM – amphibolite facies. (B) Discrimination according to mean votes of the 'setting and metamorphic facies' model of Schönig et al. (2021a). BS/GS – blueschist/greenschist facies, AM – amphibolite facies; GR – granulite facies; and EC/UHP – eclogite/ultrahigh-pressure facies. Grey bars indicate an assignment to mantle rocks. Garnet compositions of the Western Gneiss Region in Norway from Schönig et al. (2018a), of the Saxonian Erzgebirge in Germany from Schönig et al. (2019, 2020, 2021b), and the D'Entrecasteaux metamorphic complex in Papua New Guinea from Baldwin et al. (2021).

Figure 6: Prediction of metamorphic host-rock facies based on major-element composition of all individual analyses (9–20 spots per grain) for coesite- and diamond-bearing garnet grains that have not been classified as being sourced from eclogite-facies rocks in Figure 5. (A) Discrimination according

to probabilities after Tolosana-Delgado et al. (2018) using prior ‘equal-M’. EC – eclogite facies; GR – granulite facies; and AM – amphibolite facies. (B) Discrimination according to votes of the ‘setting and metamorphic facies’ model of Schönig et al. (2021a). BS/GS – blueschist/greenschist facies, AM – amphibolite facies; GR – granulite facies; and EC/UHP – eclogite/ultrahigh-pressure facies. Grey bars indicate an assignment to mantle rocks. Garnet compositions of the Western Gneiss Region in Norway from Schönig et al. (2018a), of the Saxonian Erzgebirge in Germany from Schönig et al. (2019, 2020, 2021b), and the D’Entrecasteaux metamorphic complex from Baldwin et al. (2021).

Figure 7: Discrimination results of all inclusion-bearing garnets from sample JS-Erz-14s after the ‘setting and metamorphic facies’ model after Schönig et al. (2021a). Shown are the mean votes for individual grains regarding ‘setting’ (upper diagram), ‘metamorphic facies’ (middle diagram), as well as their corresponding class assignment based on the majority vote (lower diagram). Symbols for UHP inclusion-bearing garnets are filled in bright green. IG – igneous; MS – metasomatic; MM – metamorphic; MA – mantle; BS/GS – blueschist/greenschist facies, AM – amphibolite facies; GR – granulite facies; and EC/UHP – eclogite/ultrahigh-pressure facies. Garnet compositions from Schönig et al. (2019, 2020, 2021b).

Figure 8: Photomicrograph and three-dimensional hyperspectral Raman images of coesite-bearing garnet. Garnet number 90 from sample JS-Erz-3s (cf. fig. 2A of Schönig et al., 2019). See main text for instrumental setup.

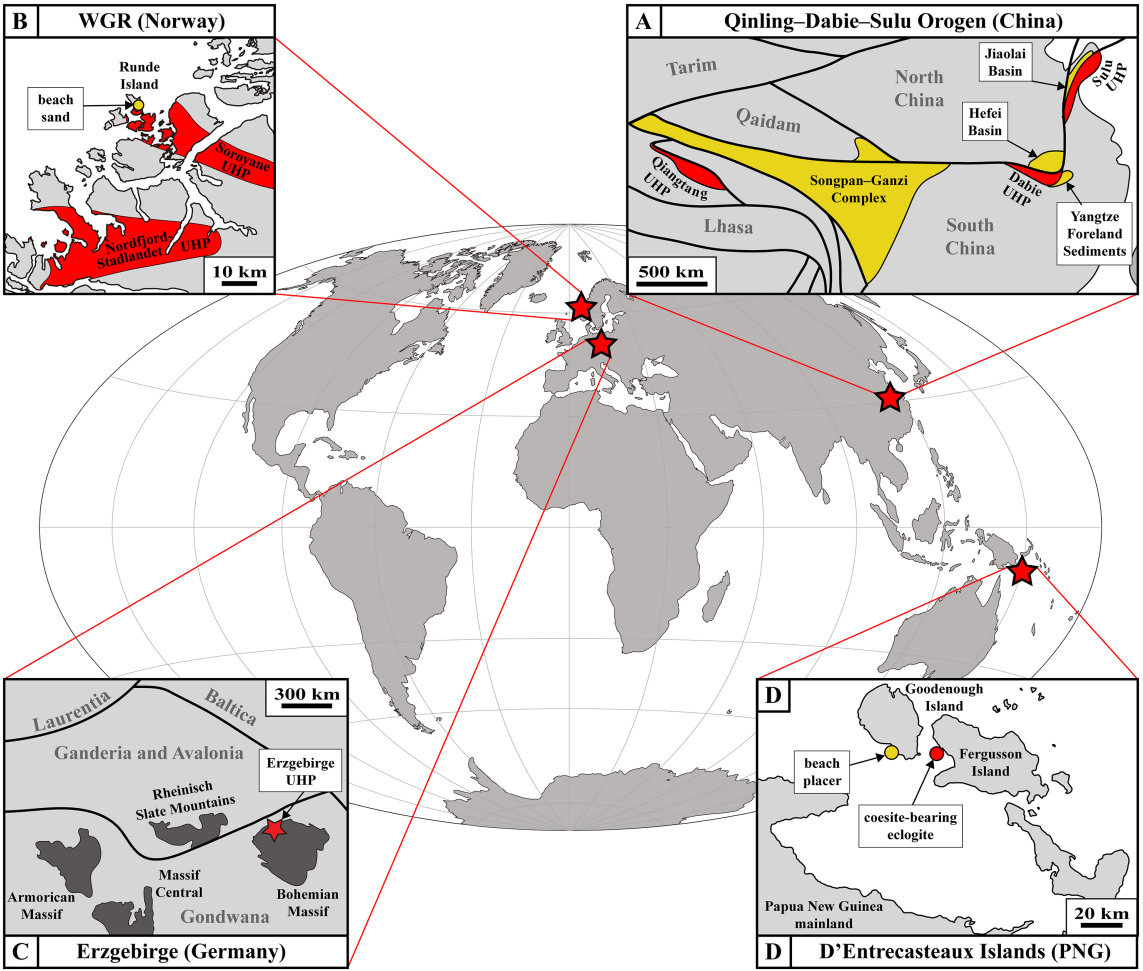
B
WGR (Norway)
Runde Island
beach sand
Sørøyane UHP
Nordfjord-Stadlandet UHP
10 km
A
Qinling–Dabie–Sulu Orogen (China)
Tarim
North China
Qaidam
Jiaolai Basin
Sulu UHP
Hefei Basin
Qiangtang UHP
Songpan–Ganzi Complex
Dabie UHP
Lhasa
South China
Yangtze Foreland Sediments
500 km
300 km
Laurentia
Baltica
Ganderia and Avalonia
Erzgebirge UHP
Rheinisch Slate Mountains
Armorican Massif
Massif Central
Bohemian Massif
Gondwana
C
Erzgebirge (Germany)
D
Goodenough Island
beach placer
Fergusson Island
coesite-bearing eclogite
Papua New Guinea mainland
20 km
D
D'Entrecasteaux Islands (PNG)

Figure 1

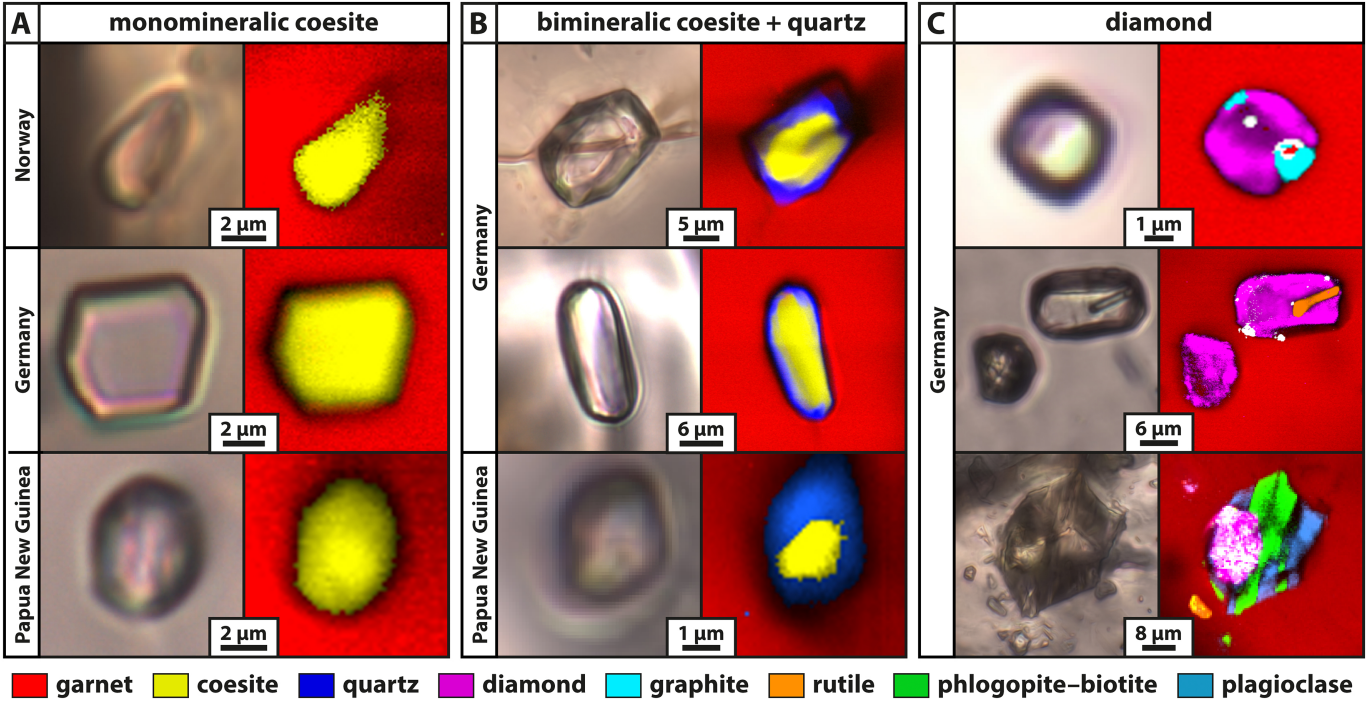
A
monomineralic coesite
B
bimineralic coesite + quartz
C
diamond
Norway
Germany
Papua New Guinea
Germany
Germany
Papua New Guinea
2 µm
2 µm
2 µm
5 µm
6 µm
1 µm
1 µm
6 µm
8 µm
garnet
coesite
quartz
diamond
graphite
rutile
phlogopite–biotite
plagioclase

Figure 2

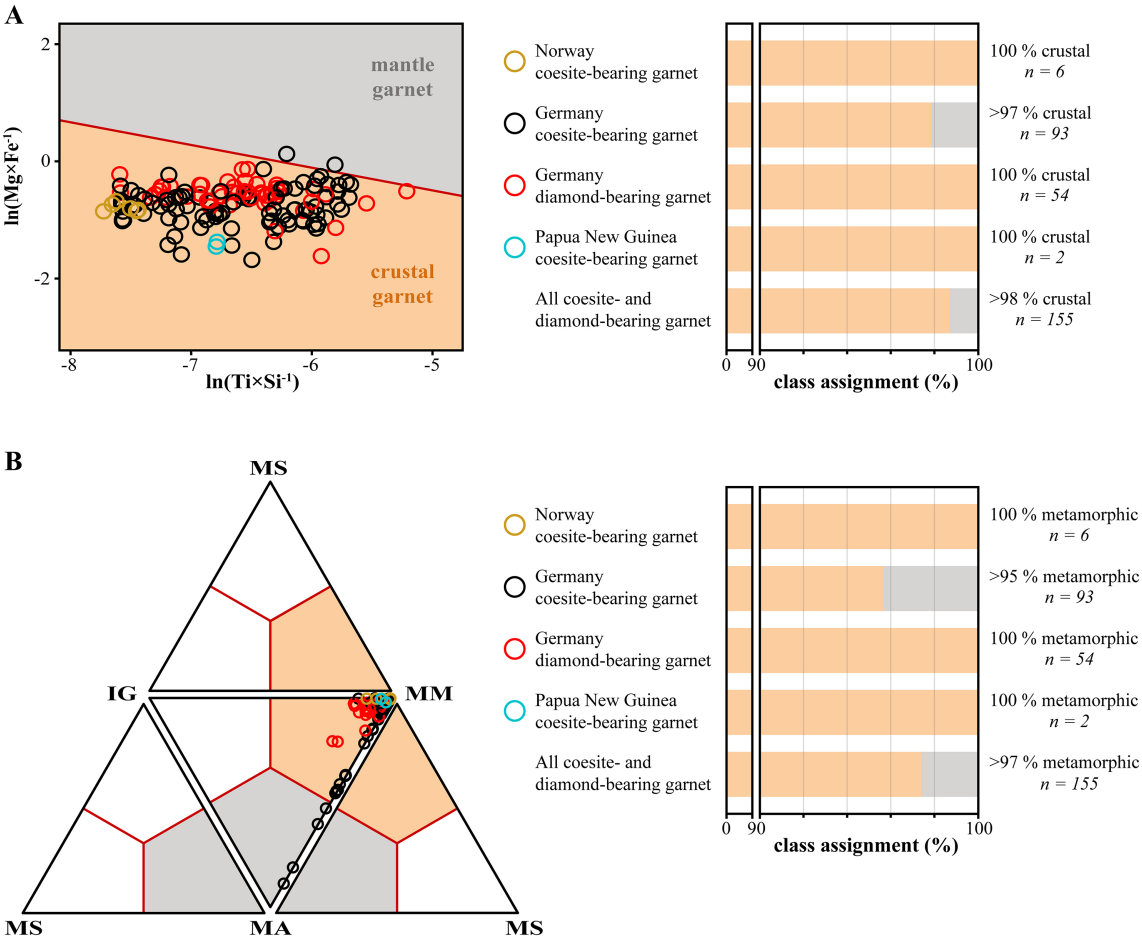
A
mantle garnet
crustal garnet
ln(Mg×Fe⁻¹)
ln(Ti×Si⁻¹)
2
0
-2
-8
-7
-6
-5
Norway coesite-bearing garnet
Germany coesite-bearing garnet
Germany diamond-bearing garnet
Papua New Guinea coesite-bearing garnet
All coesite- and diamond-bearing garnet
100 % crustal n = 6
>97 % crustal n = 93
100 % crustal n = 54
100 % crustal n = 2
>98 % crustal n = 155
0
90
100
class assignment (%)
B
MS
IG
MM
MS
MA
MS
Norway coesite-bearing garnet
Germany coesite-bearing garnet
Germany diamond-bearing garnet
Papua New Guinea coesite-bearing garnet
All coesite- and diamond-bearing garnet
100 % metamorphic n = 6
>95 % metamorphic n = 93
100 % metamorphic n = 54
100 % metamorphic n = 2
>97 % metamorphic n = 155
0
90
100
class assignment (%)

Figure 3

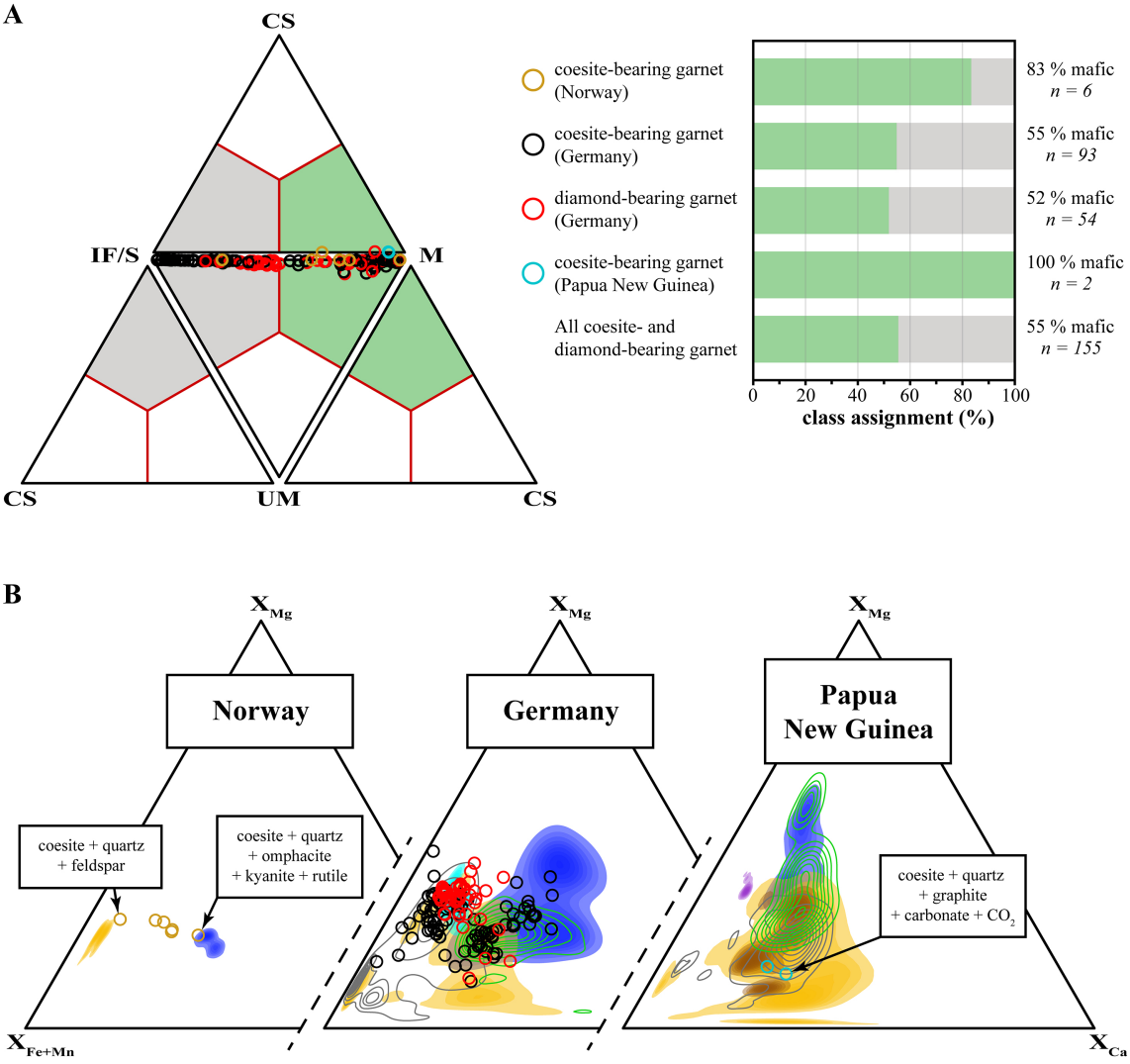
A
CS
IF/S
M
CS
UM
CS
coesite-bearing garnet (Norway)
coesite-bearing garnet (Germany)
diamond-bearing garnet (Germany)
coesite-bearing garnet (Papua New Guinea)
All coesite- and diamond-bearing garnet
83 % mafic
n = 6
55 % mafic
n = 93
52 % mafic
n = 54
100 % mafic
n = 2
55 % mafic
n = 155
0
20
40
60
80
100
class assignment (%)
B
X Mg
X Mg
X Mg
Norway
Germany
Papua New Guinea
coesite + quartz + feldspar
coesite + quartz + omphacite + kyanite + rutile
coesite + quartz + graphite + carbonate + CO2
X Fe+Mn
X Ca
garnet of local crystalline rocks
felsic gneiss
diamond-bearing felsic gneiss (Germany)
eclogite
coesite eclogite (Papua New Guinea)
retrogressed eclogite and amphibolite (Papua New Guinea)
detrital garnet
coesite bearing (Norway)
coesite bearing (Germany)
diamond bearing (Germany)
graphite bearing
omphacite bearing
coesite bearing (Papua New Guinea)

Figure 4

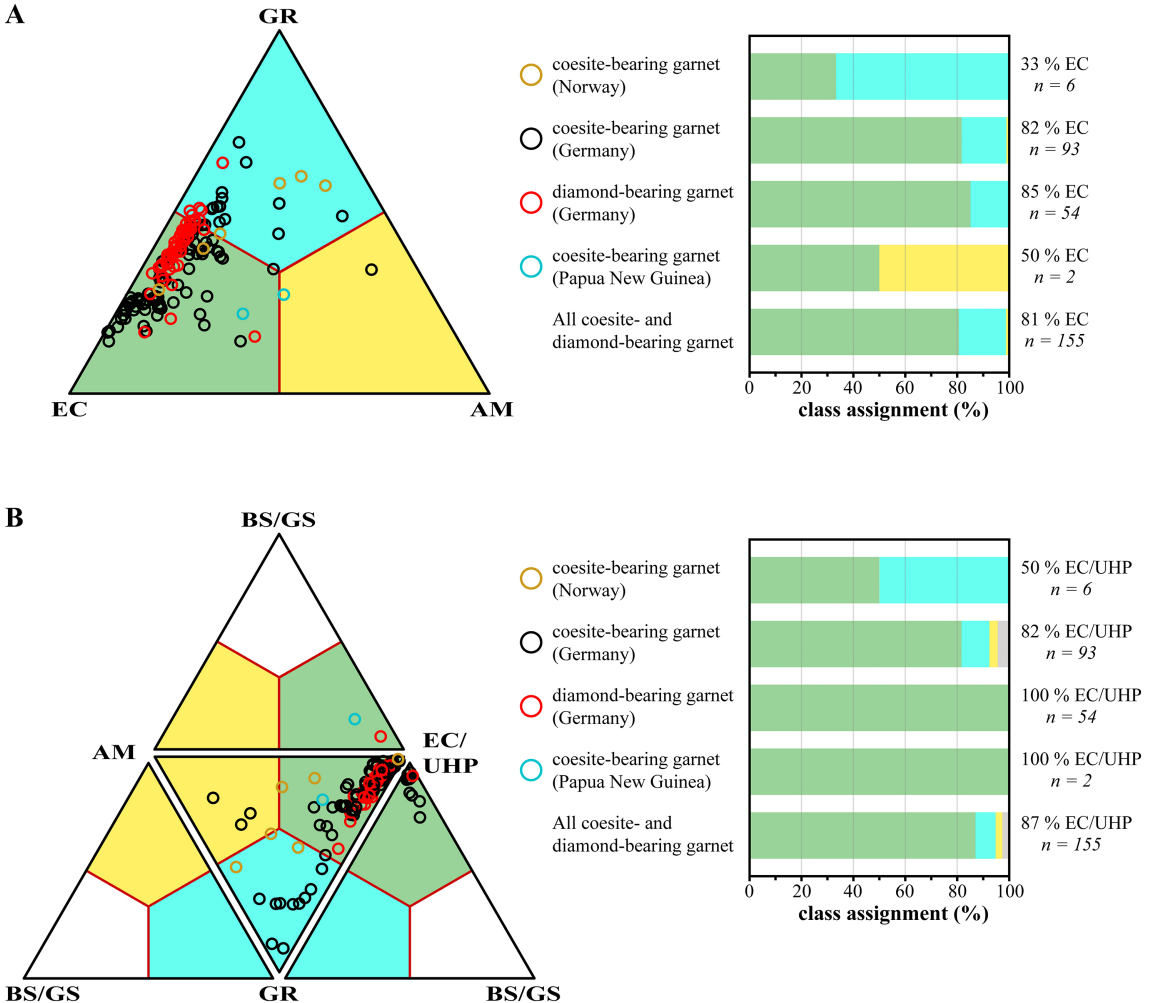
A
GR
EC
AM
coesite-bearing garnet (Norway)
coesite-bearing garnet (Germany)
diamond-bearing garnet (Germany)
coesite-bearing garnet (Papua New Guinea)
All coesite- and diamond-bearing garnet
33 % EC
n = 6
82 % EC
n = 93
85 % EC
n = 54
50 % EC
n = 2
81 % EC
n = 155
0
20
40
60
80
100
class assignment (%)
B
BS/GS
AM
EC/
UHP
BS/GS
GR
BS/GS
coesite-bearing garnet (Norway)
coesite-bearing garnet (Germany)
diamond-bearing garnet (Germany)
coesite-bearing garnet (Papua New Guinea)
All coesite- and diamond-bearing garnet
50 % EC/UHP
n = 6
82 % EC/UHP
n = 93
100 % EC/UHP
n = 54
100 % EC/UHP
n = 2
87 % EC/UHP
n = 155
0
20
40
60
80
100
class assignment (%)

Figure 5

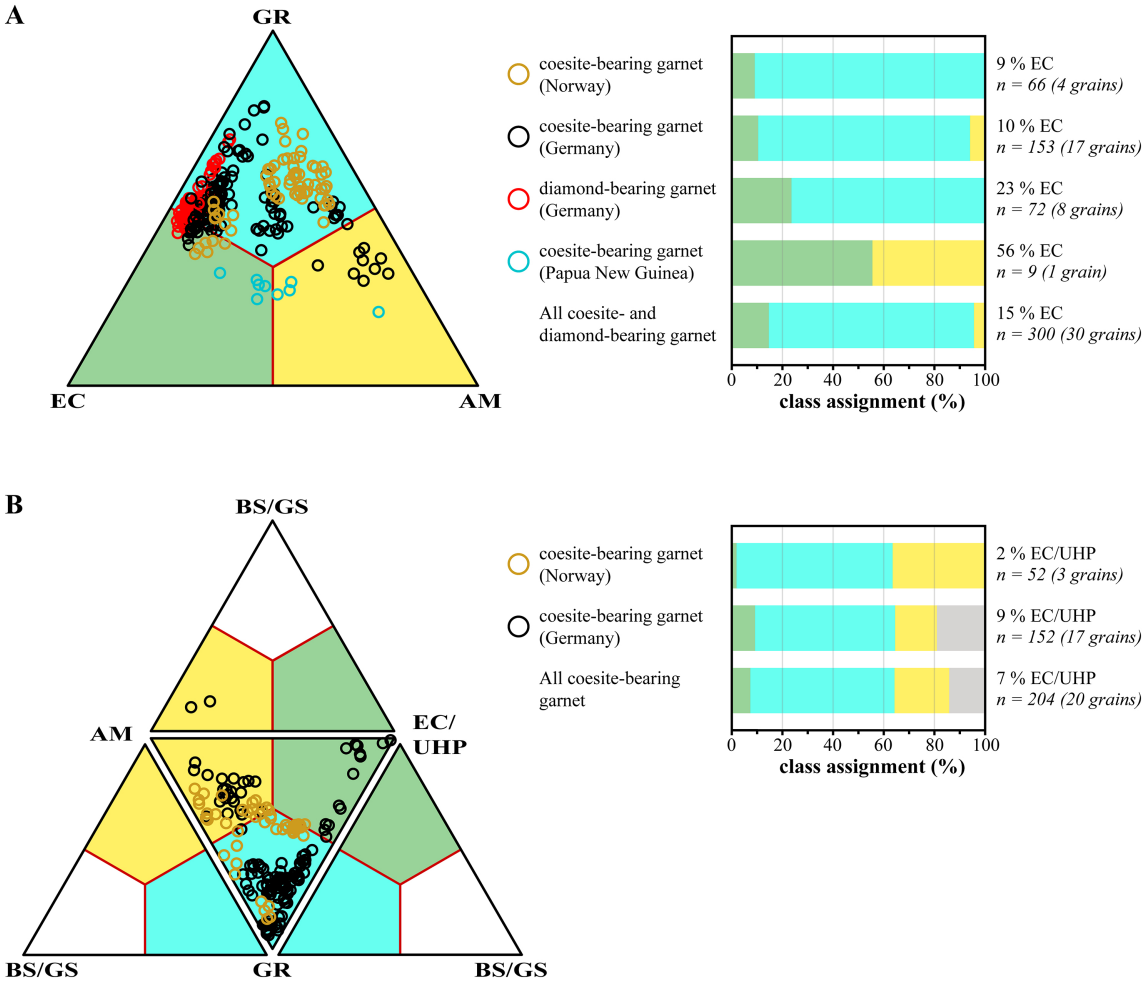
A
GR
EC
AM
coesite-bearing garnet (Norway)
coesite-bearing garnet (Germany)
diamond-bearing garnet (Germany)
coesite-bearing garnet (Papua New Guinea)
All coesite- and diamond-bearing garnet
9 % EC
n = 66 (4 grains)
10 % EC
n = 153 (17 grains)
23 % EC
n = 72 (8 grains)
56 % EC
n = 9 (1 grain)
15 % EC
n = 300 (30 grains)
0 20 40 60 80 100
class assignment (%)
B
BS/GS
AM
EC/ UHP
BS/GS
GR
BS/GS
coesite-bearing garnet (Norway)
coesite-bearing garnet (Germany)
All coesite-bearing garnet
2 % EC/UHP
n = 52 (3 grains)
9 % EC/UHP
n = 152 (17 grains)
7 % EC/UHP
n = 204 (20 grains)
0 20 40 60 80 100
class assignment (%)

Figure 6

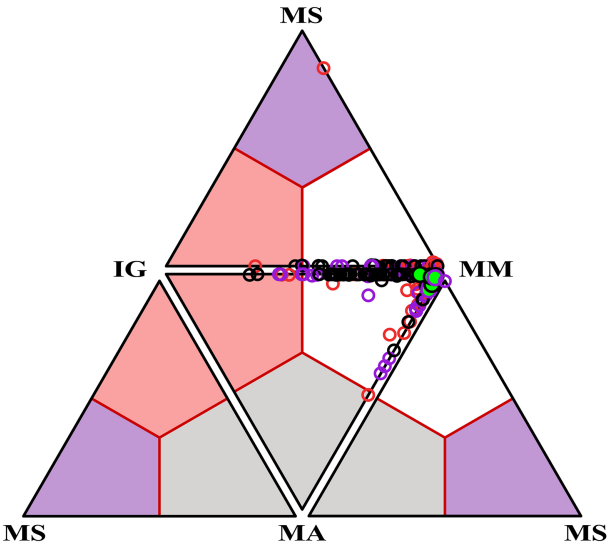
MS
IG
MM
MS
MA
MS

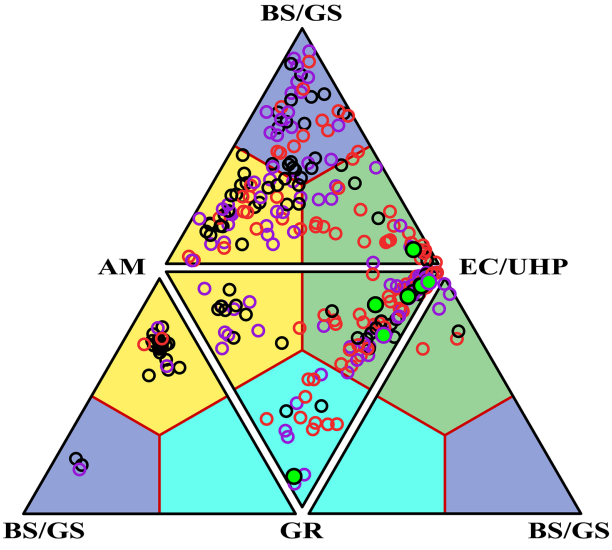
BS/GS
AM
EC/UHP
BS/GS
GR
BS/GS

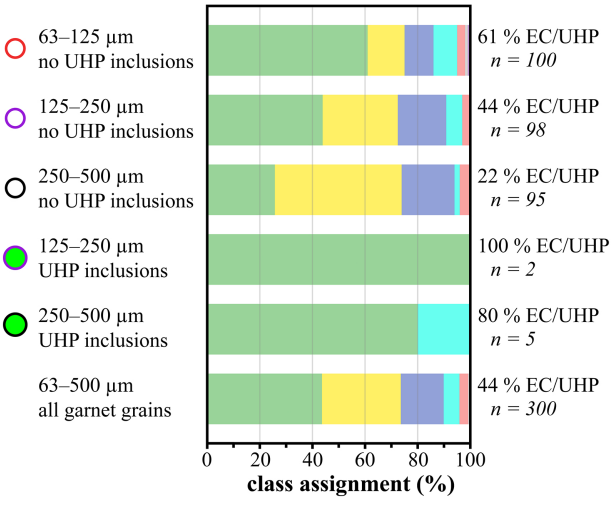
63–125 µm
no UHP inclusions
125–250 µm
no UHP inclusions
250–500 µm
no UHP inclusions
125–250 µm
UHP inclusions
250–500 µm
UHP inclusions
63–500 µm
all garnet grains
61 % EC/UHP
n = 100
44 % EC/UHP
n = 98
22 % EC/UHP
n = 95
100 % EC/UHP
n = 2
80 % EC/UHP
n = 5
44 % EC/UHP
n = 300
0
20
40
60
80
100
class assignment (%)

Figure 7

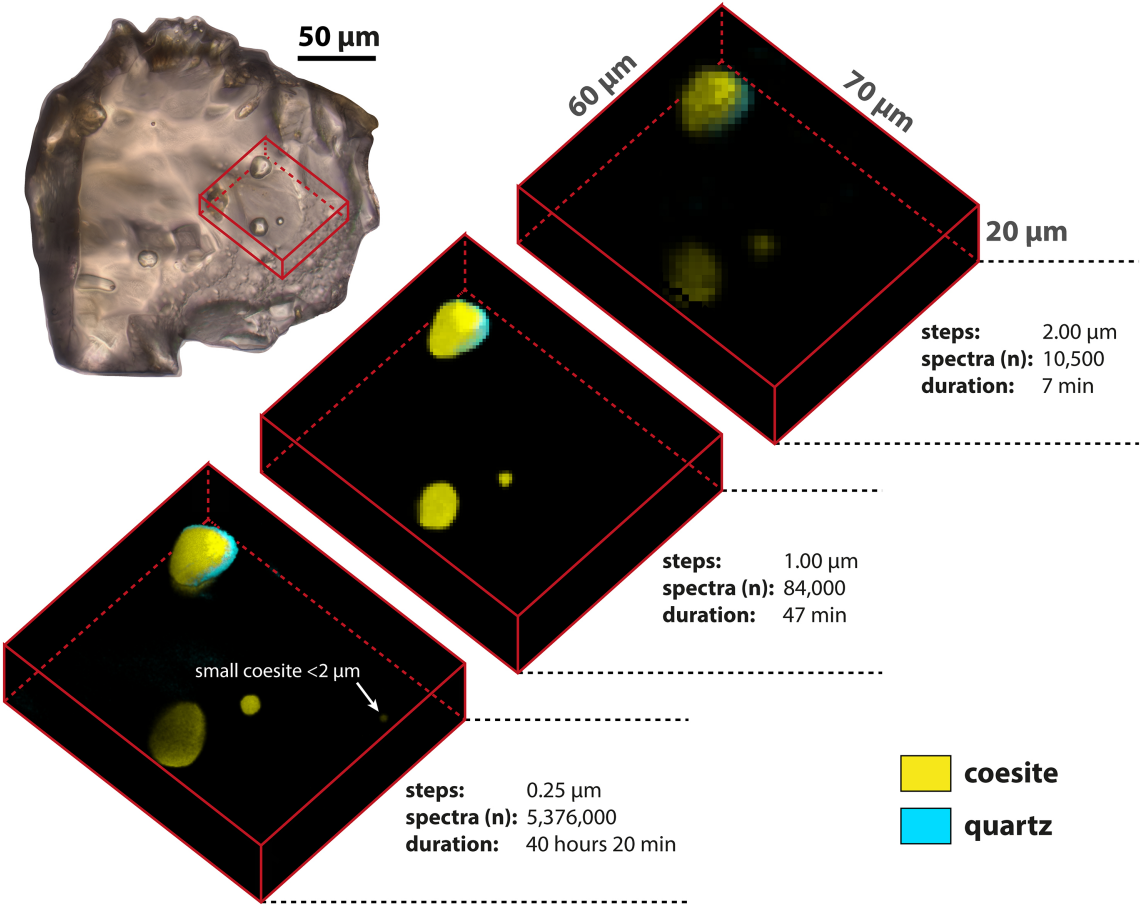
50 µm
60 µm
70 µm
20 µm
steps: 2.00 µm
spectra (n): 10,500
duration: 7 min
steps: 1.00 µm
spectra (n): 84,000
duration: 47 min
small coesite <2 µm
steps: 0.25 µm
spectra (n): 5,376,000
duration: 40 hours 20 min
coesite
quartz

Figure 8